NONLINEAR VIBRATIONS OF A CLAMPED CIRCULAR PLATE CARRYING A CONCENTRIC RIGID MASS

by

LeWayne Carl Becker

B.S., Kansas State University, 1971

A MASTER'S THESIS

Submitted in partial fulfillment of the

requirements for the degree

MASTER OF SCIENCE

Department of Mechanical Engineering

KANSAS STATE UNIVERSITY
Manhattan, Kansas

1975

Approved by

Hugh S. Walker

Major Professor

LD
2668
T4
1975
B43
c.2
Document

TABLE OF CONTENTS

LIST OF TABLES

LIST OF FIGURES

NOMENCLATURE

r, θ, z	cylindrical coordinates for the vibratory system (see Fig. 1)
h	thickness of the plate
a	outer radius of the plate
b	inner radius of the plate and the radius of the concentric rigid core
M	mass of the rigid core
t	time variable
u, w	radial and transverse displacements of the middle plane, respectively
$\varepsilon_r, \varepsilon_\theta$	radial and circumferential strains, respectively
$\sigma_r, \sigma_\theta, \sigma_z$	radial, circumferential and normal stresses, respectively
E, ν	elastic modulus and Poisson's ratio, respectively
N_r, N_θ	radial and circumferential membrane forces per unit length, respectively
M_r, M_θ	radial and circumferential bending moments per unit length, respectively
D	flexural Rigidity
U_1	strain energy due to bending
U_2	Strain energy due to stretching of the middle plane
$\varepsilon_r^o, \varepsilon_\theta^o$	radial and circumferential strains acting on the middle plane, respectively
T_1, T_2	kinetic energy of the plate and of concentric rigid mass, respectively
ρ	mass density of the plate
I	action integral for the vibrating system
δI	first variation of I
η, ζ	arbitrary functions in the admissable variations of w and u, respectively

ε	arbitrary infinitesimal constant
ψ, ϕ	stress functions
χ	dimensionless transverse displacement
ξ, τ	dimensionless space and time variables, respectively
R	radius ratio
γ	mass ratio
A, α	amplitude parameters
$g(\xi), f(\xi)$	shape functions of vibration
ω	nondimensional angular frequency
$\delta\chi$	first variation of χ
δW	virtual work of transverse forces
λ	nonlinear eigenvalue
$\bar{Y}, \bar{Z}, \bar{H}$	(6x1) vector functions
(M),(N)	coefficient matrices
$\bar{\eta}$	adjustable data in the initial value problem
(J_1)	Jacobian matrix
W_R	deflection at $\xi = R$
ω_ℓ	linear angular frequency
Ω	frequency in cycles per second

Note: With the exceptions defined above, a variable subscripted i times indicates the ith partial derivative of that variable with respect to the subscript. Examples:

$$w_r = \frac{\partial w}{\partial r} \quad , \quad \chi_{\tau\tau} = \frac{\partial^2 \chi}{\partial \tau^2} \quad , \quad g_{\xi\xi\xi\xi} = \frac{\partial^4 g}{\partial \xi^4}$$

INTRODUCTION

Circular plates with attached concentric rigid masses are common structural elements used in mechanical designs. With the advent of these modern plate and mass components being subjected to large amplitude flexural vibrations, the classical linear theory for small deflections no longer provides an accurate analysis of such systems. Thus, in many engineering applications, a more precise solution is of increasing practical importance.

When the amplitude of vibration approaches the thickness of the plate, a more rigorous analysis is required, and the effects of straining of the middle plane must be included. Consideration of this membrane effect results in a set of two equations commonly known as von Karman's Dynamic equations [1]. These two equations are coupled, fourth order, nonlinear, partial differential equations for which the only present known means of solution is by approximate methods.

Utilizing various approximate methods, many authors have investigated the large amplitude vibration characteristics of circular plates of constant thickness. However, the addition of a concentric rigid mass to the plate has received very limited attention.

By neglecting the terms of the second strain invariant, Berger [2] approximated von Karman's equations, uncoupled the two complex expressions and simplified their solution. Berger noted that the error resulting from not satisfying the equilibrium equations was insignificant in the static small deflection case, but one should expect it to have a large effect on the membrane stresses.

Handelman and Cohen [3] obtained the characteristic frequencies of a clamped circular plate carrying a rigidly attached, concentric rigid mass.

Utilizing a minimum principle, small amplitude vibration response curves were obtained for various mass and radii ratios. Extending the problem, Chiang and Chen [4] applied the Berger type equations and a modified Galerkin method to predict the large amplitude natural frequencies of circular plates with concentric rigid parts at the centers. Nowinski and Ohnabe [5] cautioned that Berger's approach to nonlinear theory, in which the elastic energy due to the second strain invariant is neglected, might lead to grave inaccuracies and even become meaningless if the boundary conditions do not restrain the edge of the plate from in-plane motions. Recently, investigating the nonlinear vibrations of a rectangular plate carrying a concentrated mass, Ramachandran [6] employed the more rigorous von Karman equations and demonstrated that Berger's approximation gives higher values for the nonlinear frequencies.

Approximate solutions are commonly obtained by separating the dependent variables, assuming a form for the space coordinate functions, and eliminating the space coordinate from the governing differential equations. An alternate approach has been recently proposed by Sandman and Huang [7]. The large amplitude vibrations of flat circular and annular plates were investigated by assuming the existance of harmonic oscillations in the form of a time coordinate function and eliminating the time variable from the equations.

This thesis is an extension of the techniques employed by Huang and Sandman to the problem of large amplitude axisymmetric vibrations of clamped flat circular plates of constant thickness carrying a rigid concentric mass. Energy methods are utilized to derive the von Karman form of the governing differential equations and the associated boundary conditions. Harmonic oscillations are assumed and through the application of a Kantorovich time averaging method, the time variable is eliminated. The resulting governing differential equations form a nonlinear eigenvalue problem whose numerical solution is obtained through consideration of the corresponding initial-value problem.

The nonlinear vibration characteristics are investigated for various mass and radii ratios, and the results agree with those of the classical linear solution when the amplitude of vibration tends to zero. Agreement with prior work is also obtained for large amplitude vibrations of a flat circular plate when the radius of the concentric rigid mass tends to zero and a mass ratio of unity is prescribed. Experimental observations of the behavior of the plate-mass system also support the method of solution. A comparison with prior results obtained using Berger's simplified equations reveals notable differences in the nonlinear frequencies predicted by the two methods.

THIS BOOK CONTAINS NUMEROUS PAGES WITH DIAGRAMS THAT ARE CROOKED COMPARED TO THE REST OF THE INFORMATION ON THE PAGE.

THIS IS AS RECEIVED FROM CUSTOMER.

DERIVATION OF THE GOVERNING EQUATIONS

Consider the thin uniform circular plate with a concentric rigid mass shown in Fig. 1. The origin of the cylindrical coordinates r, θ and z is located at the center of the undeformed middle plane.

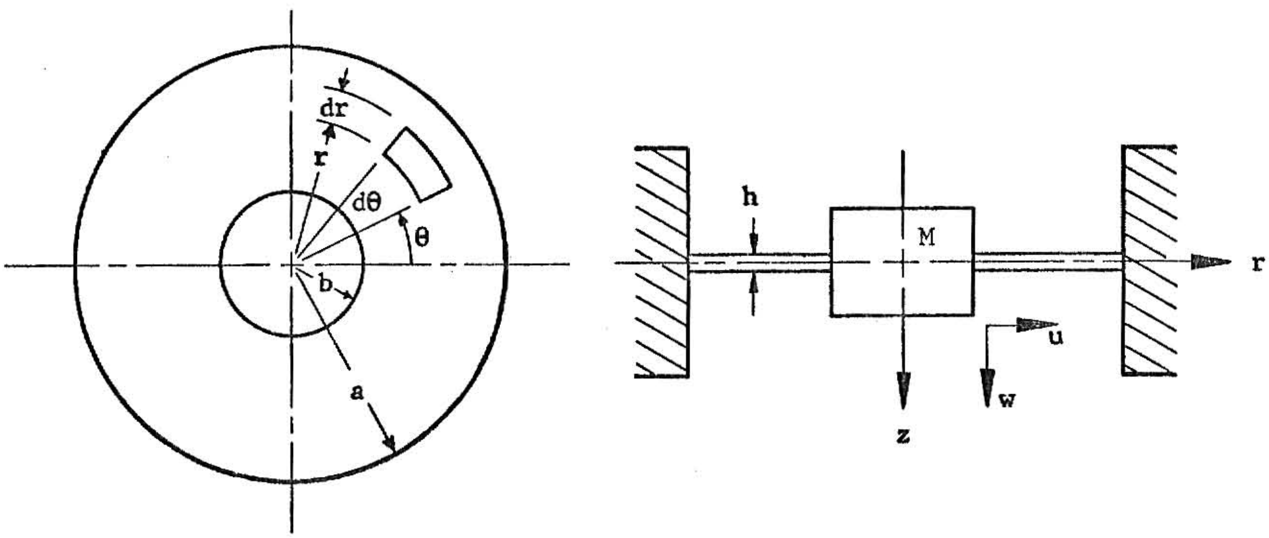

Fig. 1

The annular plate is assumed to be an elastic homogeneous and isotropic material bounded by the planes $z = \pm h/2$. It has a clamped immovable outer edge of radius a, and its inner edge is rigidly connected to the concentric mass M at radius b. The derivation of the governing equations of motion is based on the following assumptions:

(i) Normals to the middle plane of the undeformed plate remain straight and normal to the middle plane after bending.

(ii) Normal stresses, σ_z, may be neglected as they are small compared to the other stress components.

(iii) Circular symmetry with respect to the z-axis is maintained during vibration.

(iv) The effects of stretching the middle plane of the plate are not negligible.

The radial and circumferential strain-displacement relations are derived from large deflection theory as

$$\varepsilon_r = u_r + \frac{1}{2} w_r^2 - z w_{rr} \tag{1a}$$

$$\varepsilon_\theta = \frac{u}{r} - \frac{z}{r} w_r \tag{1b}$$

where u(r,t) and w(r,t) denote the radial and transverse components of the mid-plane displacement, respectively [1,8], while the subscripted variables w_r and w_{rr} represent the first and second partial derivatives of w with respect to r. The same convention is used to denote partial derivatives of the radial component of displacement and partial derivatives with respect to time.

From Hooke's laws, the stress-strain relationships are

$$\sigma_r = \frac{E}{1-\nu^2} (\varepsilon_r + \nu\varepsilon_\theta) \tag{2a}$$

$$\sigma_\theta = \frac{E}{1-\nu^2} (\varepsilon_\theta + \nu\varepsilon_r) \tag{2b}$$

where σ_r and σ_θ are the radial and circumferential stresses, respectively.

Integrating the in-plane stresses over the plate thickness, the bending moments per unit length are found to be

$$M_r = \int_{-h/2}^{h/2} \sigma_r z dz = -D[w_{rr} + \frac{\nu}{r} w_r] \tag{3a}$$

$$M_\theta = \int_{-h/2}^{h/2} \sigma_\theta z dz = -D[\frac{1}{r} w_r + \nu w_{rr}] \tag{3b}$$

and the tensile forces per unit length are

$$N_r = \int_{-h/2}^{h/2} \sigma_r dz = \frac{12D}{h^2} [u_r + \frac{1}{2} w_r^2 + \nu \frac{u}{r}] \tag{4a}$$

$$N_\theta = \int_{-h/2}^{h/2} \sigma_\theta dz = \frac{12D}{h^2} [\frac{u}{r} + \nu u_r + \frac{\nu}{2} w_r^2] \tag{4b}$$

where

$$D = \frac{Eh^3}{12(1-\nu^2)}$$

is the flexural rigidity of the plate.

The strain energy of bending is found as [1,8]

$$U_1 = - \int_o^{2\pi} \int_b^a \left[\frac{M_r w_{rr}}{2} + \frac{M_\theta w_r}{2r} \right] r dr d\theta$$

Substitution of M_r and M_θ from expressions (3) into the above equation gives the strain energy due to bending in terms of the displacements

$$U_1 = \pi D \int_b^a [w_{rr}^2 + 2 \frac{\nu}{r} w_r w_{rr} + \frac{1}{r^2} w_r^2] r dr \tag{5}$$

The strain energy due to stretching of the middle plane is [1,8]

$$U_2 = \int_o^{2\pi} \int_b^a \left[\frac{N_r \varepsilon_r^o}{2} + \frac{N_\theta \varepsilon_\theta^o}{2} \right] r dr d\theta$$

where

$$\varepsilon_r^o = u_r + \frac{1}{2} w_r^2$$

and

$$\varepsilon_\theta^o = \frac{u}{r}$$

are the strain components acting on the middle plane of the plate. Substituting N_r and N_θ from Eq. (4) and integrating yields the strain energy due to stretching of the middle plane as

$$U_2 = \frac{12\pi D}{h^2}\int_b^a \left[u_r^2 + u_r w_r^2 + \frac{1}{4} w_r^4 + \nu \frac{u}{r}(2u_r + w_r^2) + \frac{u^2}{r^2}\right] r dr \tag{6}$$

Considering only the transverse component of velocity, the kinetic energy of the plate is given by

$$T_1 = \frac{\rho h}{2}\int_o^{2\pi}\int_b^a w_t^2 r dr d\theta$$

where ρ denotes the mass per unit volume of the plate. Integration yields

$$T_1 = \pi h \rho \int_b^a w_t^2 r dr \tag{7}$$

The kinetic energy of the concentric rigid mass is

$$T_2 = \frac{1}{2} M w_t^2 \Big|_{r=b} \tag{8}$$

Hamilton's principle requires that the first variation $\delta I = 0$, where the action integral I is defined by

$$I = \int_{t_o}^{t_1} (T_1 + T_2 - U_1 - U_2) dt \tag{9}$$

Substitution of Eqs. (5), (6), (7) and (8) into Eq. (9) yields an expression of the form

$$I = \int_{t_o}^{t_1}\left[\pi \int_b^a f^*(r,t;w,u,w_r,w_{rr},u_r,w_t) dr - g^*(r{=}b,t;w_t)\right] dt$$

where the function f^* is defined by

$$f^* = \rho h r w_t^2 - D[r w_{rr}^2 + 2\nu w_r w_{rr} + \frac{1}{r} w_r^2] - \frac{12D}{h^2}[r u_r^2 + r u_r w_r^2$$

$$+ \frac{r}{4} w_r^4 + 2\nu u u_r + \nu u w_r^2 + \frac{u^2}{r}]$$

and the function g^* is

$$g^* = \frac{1}{2} M w_t^2 \Big|_{r=b}$$

The displacement functions w(r,t) and u(r,t) are given the admissable variations $\varepsilon\eta(r,t)$ and $\varepsilon\zeta(r,t)$, where ε is an arbitrary infinitesimal constant while $\eta(r,t)$ and $\zeta(r,t)$ are any continuously differentiable functions which satisfy the forced boundary conditions. Then I takes an increment ΔI determined by

$$\Delta I = \int_{t_o}^{t_1} \left[\left\{ \pi \int_b^a f^*(r,t;w+\varepsilon\eta, u+\varepsilon\zeta, w_r+\varepsilon\eta_r, w_{rr}+\varepsilon\eta_{rr}, u_r+\varepsilon\zeta_r, w_t+\varepsilon\eta_t) - f^* \right\} dr - \{g^*(r,t;w_t+\varepsilon\eta_t) - g^*\} \right] dt$$

Expanding the integrand accordingly, integrating by parts, and retaining only that part of ΔI which is linear in ε, the first variation δI is obtained. The resulting expression is listed in Appendix A. Extremization of the functional I is completed by observing the necessary condition that the integrands of the double integrals and the single integrals vanish separately. Thus, the double integrals provide the governing equations of motion,

$$D[w_{rrrr} + \frac{2}{r} w_{rrr} - \frac{1}{r^2} w_{rr} + \frac{1}{r^3} w_r] + \rho h w_{tt} = \frac{12D}{h^2} [u_r w_{rr} + u_{rr} w_r + \frac{1}{r} u_r w_r + \frac{3}{2} w_r^2 w_{rr} + \frac{1}{2r} w_r^3 + \frac{\nu}{r} (u w_{rr} + u_r w_r)] \tag{10a}$$

$$u_{rr} + \frac{1}{r} u_r - \frac{u}{r^2} + w_r w_{rr} + \frac{1}{2r} w_r^2 - \frac{\nu}{2r} w_r^2 = 0 \tag{10b}$$

while the single integrals provide the natural boundary conditions;

$$2\pi D r [w_{rr} + \frac{\nu}{r} w_r] \eta_r \Big|_b^a = 0 \tag{11}$$

$$\frac{24\pi D}{h^2} r\left[u_r + \frac{w_r^2}{2} + \frac{\nu u}{r}\right]\zeta\Big|_b^a = 0$$

$$2\pi Dr\left[w_{rrr} + \frac{w_{rr}}{r} - \frac{w_r}{r^2}\right]\eta\Big|_b^a - \frac{24\pi D}{h^2} rw_r[u_r + \frac{1}{2}w_r^2 + \nu\frac{u}{r}]\ \eta\Big|_b^a - [Mw_{tt}]\eta\Big|_b = 0$$

The appropriate geometric boundary conditions for a clamped circular plate carrying a concentric rigid mass are

$$w|_{r=a} = 0 \qquad w_r|_{r=b} = 0$$

$$w_r|_{r=a} = 0 \qquad u|_{r=b} = 0$$

$$u|_{r=a} = 0 \tag{12}$$

Forcing the geometric boundary conditions on the conditions (11) provides the following set of boundary conditions to be satisfied

$$w|_{r=a} = 0 \qquad w_r|_{r=b} = 0$$

$$w_r|_{r=a} = 0 \qquad u|_{r=b} = 0 \tag{13}$$

$$u|_{r=a} = 0 \qquad [w_{rrr} + \frac{1}{r}w_{rr} - \frac{1}{r^2}w_r]|_{r=b} = -\frac{M}{2\pi bD}w_{tt}|_{r=b}$$

The stress function $\psi(r,t)$ is introduced by using the following relations

$$\frac{\psi}{r} = N_r \qquad \frac{\partial\psi}{\partial r} = N_\theta \tag{14}$$

which transform the governing differential Eqs. (10a) and (10b) into

$$\frac{D}{r}[r\{\frac{1}{r}(rw_r)_r\}_r]_r + \rho hw_{tt} - \frac{1}{r}(\psi w_r)_r = 0 \tag{15a}$$

and

$$\psi_{rr} + \frac{1}{r}\psi_r - \frac{1}{r^2}\psi = -\frac{Eh}{2r}(w_r)^2 \tag{15b}$$

For mathematical tractability, the following non-dimensional variables are introduced

$$\chi = w/a \qquad \xi = r/a \qquad R = b/a$$

$$\phi = \frac{\psi}{Eha} \qquad \gamma = \frac{M}{\pi b^2 \rho h} \qquad \tau = t\left(\frac{D}{\rho h a^4}\right)^{1/2}$$

The governing Eqs. (15a) and (15b) thus become

$$\chi_{\xi\xi\xi\xi} + \frac{2}{\xi}\chi_{\xi\xi\xi} - \frac{1}{\xi^2}\chi_{\xi\xi} + \frac{1}{\xi^3}\chi_\xi + \chi_{\tau\tau} = \frac{12}{\xi}(1-\nu^2)\left(\frac{a}{h}\right)^2[\chi_\xi\phi]_\xi \tag{16a}$$

and

$$\phi_{\xi\xi} + \frac{1}{\xi}\phi_\xi - \frac{1}{\xi^2}\phi + \frac{1}{2\xi}\chi_\xi^2 = 0 \tag{16b}$$

Following the introduction of the stress function and the dimensionless parameters, the boundary conditions (13) take the alternate form

$$\begin{aligned} &(\chi)_{\xi=1} = 0 && (\chi_\xi)_{\xi=R} = 0 \\ &(\chi_\xi)_{\xi=1} = 0 && (\phi_\xi - \tfrac{\nu}{\xi}\phi)_{\xi=R} = 0 \\ &(\phi_\xi - \tfrac{\nu}{\xi}\phi)_{\xi=1} = 0 && (\chi_{\xi\xi\xi} + \tfrac{1}{\xi}\chi_{\xi\xi} - \tfrac{1}{\xi^2}\chi_\xi + \tfrac{\xi}{2}\gamma\chi_{\tau\tau})_{\xi=R} = 0 \end{aligned} \tag{17}$$

where the outer radius has been normalized to simplify the numerical computations and provide generalized results.

APPROXIMATE ANALYSIS

A solution to the problem defined by the nonlinear differential equations (16a) and (16b) must satisfy the boundary conditions (17). Lack of an explicit solution to the problem posed necessitates the use of an approximate method and minimization of the inherent error. The Ritz-Kantorovich averaging method [7,9], which has been successfully applied to numerous elasticity problems [9,10], is adopted to eliminate the time variable and reduce the governing differential equations to a system of ordinary differential equations.

Proceeding accordingly by assuming the existance of harmonic oscillations, the plate behavior is represented by

$$\chi(\xi,\tau) = A\ g(\xi)\ \sin \omega\tau \tag{18a}$$

$$\phi(\xi,\tau) = A^2 f(\xi)\ \sin^2 \omega\tau \tag{18b}$$

where A is an amplitude parameter, ω is the angular frequency, and $g(\xi)$ and $f(\xi)$ are shape functions to be determined.

Since $\phi(\xi,\tau)$ is associated with the radial displacement function $u(r,t)$, it should assume the same value for positive and negative transverse deflections of the plate. Hence, equation (18b) follows from assumption (18a).

Substitution of Eqs. (18) into the governing differential Eq. (16b) yields

$$f_{\xi\xi} + \frac{1}{\xi} f_\xi - \frac{1}{\xi^2} f + \frac{1}{2\xi} (g_\xi)^2 = 0 \tag{19}$$

Although Eqs. (18) do not satisfy the differential Eq. (16a) for all τ, the residual may be found and minimized by the Ritz-Kantorovich method. At any instant, the virtual work of all transverse forces as they move through a virtual displacement $\delta\chi = A\ \delta g \sin \omega\tau$ is

$$\delta W = \int_R^1 [\chi_{\xi\xi\xi\xi} + \frac{2}{\xi}\chi_{\xi\xi\xi} - \frac{1}{\xi^2}\chi_{\xi\xi} + \frac{1}{\xi^3}\chi_\xi + \chi_{\tau\tau}$$

$$- \frac{12}{\xi}(1-\nu^2)\left(\frac{a}{h}\right)^2 (\chi_\xi\phi)_\xi]\delta\chi\xi d\xi \tag{20}$$

Equating the average virtual work over one complete period of oscillation to zero [11], that is,

$$\int_0^{\frac{2\pi}{\omega}} (\delta W)d\tau = 0 \tag{21}$$

and substituting expressions (18) into Eq. (20) and then into (21) yields upon integration with respect to τ;

$$g_{\xi\xi\xi\xi} + \frac{2}{\xi}g_{\xi\xi\xi} - \frac{1}{\xi^2}g_{\xi\xi} + \frac{1}{\xi^3}g_\xi - \lambda g - 9(1-\nu^2)\frac{\alpha}{\xi}(g_\xi f)_\xi = 0 \tag{22}$$

where $\alpha = \left(\frac{Aa}{h}\right)^2$ and $\lambda = \omega^2$ are additional dimensionless parameters related to the amplitude and the angular frequency, respectively. Hence the time variable is eliminated from the governing differential equations with an average minimum error over one cycle of the assumed motion, and the assumed harmonic motion becomes governed by the pair of ordinary nonlinear differential Eqs. (19) and (22).

A similar transformation of the boundary conditions (17) yields

$$\begin{aligned} &(g)_{\xi=1} = 0 && (g_\xi)_{\xi=R} = 0 \\ &(g_\xi)_{\xi=1} = 0 && (f_\xi - \frac{\nu}{\xi}f)_{\xi=R} = 0 \\ &(f_\xi - \frac{\nu}{\xi}f)_{\xi=1} = 0 && (f_{\xi\xi\xi} + \frac{1}{\xi}g_{\xi\xi} - \frac{1}{\xi^2}g_\xi - \frac{\xi}{2}\gamma\lambda g)_{\xi=R} = 0 \end{aligned} \tag{23}$$

In addition, by imposing the normalization condition

$$(g)_{\xi=R} = 1\ . \tag{24}$$

a unique relationship between the parameters α and λ is assured.

Finally, Eqs. (19), (22), (23) and (24) form a nonlinear eigenvalue problem which characterizes the large amplitude axisymmetric vibrations of a clamped circular plate with a concentric rigid mass attached. Summarizing;

$$g_{\xi\xi\xi\xi} + \frac{2}{\xi} g_{\xi\xi\xi} - \frac{1}{\xi^2} g_{\xi\xi} + \frac{1}{\xi^3} g_\xi - \lambda g - 9(1-\nu^2) \frac{\alpha}{\xi} (g_\xi f)_\xi = 0 \tag{25a}$$

$$f_{\xi\xi} + \frac{1}{\xi} f_\xi - \frac{1}{\xi^2} f + \frac{1}{2\xi} (g_\xi)^2 = 0 \tag{25b}$$

$$(g)_{\xi=1} = 0 \qquad (g)_{\xi=R} = 1 \tag{25c}$$

$$(g_\xi)_{\xi=1} = 0 \qquad (g_\xi)_{\xi=R} = 0$$

$$(f_\xi - \frac{\nu}{\xi} f)_{\xi=1} = 0 \qquad (f_\xi - \frac{\nu}{\xi} f)_{\xi=R} = 0$$

$$(g_{\xi\xi\xi} + \frac{1}{\xi} g_{\xi\xi} - \frac{1}{\xi^2} g_\xi - \frac{\xi}{2} \gamma\lambda g)_{\xi=R} = 0$$

METHOD OF SOLUTION

The nonlinear eigenvalue problem formed by Eqs. (25a) and (25b), along with the boundary conditions (25c), may be solved through the application of numerical integration to the associated initial value problem. The problem is reformulated by reducing the governing Eqs. (25a) and (25b) to an equivalent system of six first order equations,

$$\frac{d\bar{Y}}{d\xi} = \bar{H}(\xi,\bar{Y};\lambda,\alpha,\gamma) \qquad R \leq \xi \leq 1 \tag{26a}$$

where the components of $\bar{Y}$ are defined as

$$\bar{Y}(\xi) = \begin{Bmatrix} g \\ g_\xi \\ g_{\xi\xi} \\ g_{\xi\xi\xi} \\ f \\ f_\xi \end{Bmatrix} = \begin{Bmatrix} y_1 \\ y_2 \\ y_3 \\ y_4 \\ y_5 \\ y_6 \end{Bmatrix}$$

and the components of the (6x1) vector function $\bar{H}$ are

$$\bar{H} = \begin{Bmatrix} y_2 \\ y_3 \\ y_4 \\ -\frac{2}{\xi} y_4 + \frac{1}{\xi^2} y_3 - \frac{1}{\xi^3} y_2 + \lambda y_1 + 9(1-\nu^2)\,\frac{\alpha}{\xi}\,(y_2 y_6 + y_3 y_5) \\ y_6 \\ -\frac{1}{\xi} y_6 + \frac{1}{\xi^2} y_5 - \frac{1}{2\xi}(y_2)^2 \end{Bmatrix}$$

The boundary and normalization conditions of (25c) may be expressed as

$$(M)\bar{Y}(R) = \begin{Bmatrix} 1 \\ 0 \\ 0 \\ 0 \end{Bmatrix} \tag{26b}$$

and

$$(N)\bar{Y}(1) = \begin{Bmatrix} 0 \\ 0 \\ 0 \end{Bmatrix} \tag{26c}$$

where (M) and (N) are the matrices

$$(M) = \begin{pmatrix} 1 & 0 & 0 & 0 & 0 & 0 \\ 0 & 1 & 0 & 0 & 0 & 0 \\ -\frac{R}{2}\gamma\lambda & -\frac{1}{R^2} & \frac{1}{R} & 1 & 0 & 0 \\ 0 & 0 & 0 & 0 & -\frac{\nu}{R} & 1 \end{pmatrix}$$

and

$$(N) = \begin{pmatrix} 1 & 0 & 0 & 0 & 0 & 0 \\ 0 & 1 & 0 & 0 & 0 & 0 \\ 0 & 0 & 0 & 0 & -\nu & 1 \end{pmatrix}$$

in which the rows of (M) and (N) are determined from the boundary conditions, and the first row of (M) is $y_1(R) = 1$, the normalizing condition at the junction of the plate and rigid mass. The remaining rows of (M) define the conditions of zero slope, zero radial deflection, and equate the shear force at the inner boundary to d'Alembert's force of the rigid mass. Likewise, the rows of (N) define the boundary conditions of zero transverse deflection, slope and radial deflection at the outer boundary of the circular plate, ξ=1.

INITIAL VALUE PROBLEM

An approximate numerical solution to the reduced eigenvalue problem given by the system of Eqs. (26) is facilitated by introducing the initial value problem

$$\frac{d\bar{Z}}{d\xi} = \bar{H}(\xi,\bar{Z};\alpha,\lambda,\gamma) \tag{27a}$$

$$\bar{Z}(R) = \begin{Bmatrix} z_1 \\ z_2 \\ z_3 \\ z_4 \\ z_5 \\ z_6 \end{Bmatrix}_{\xi=R} = \begin{Bmatrix} 1 \\ 0 \\ \eta_1 \\ -\frac{\eta_1}{R} + \frac{R}{2}\gamma\lambda \\ \eta_2 \\ \frac{\nu}{R}\eta_2 \end{Bmatrix} \tag{27b}$$

where $\bar{Z}(R)$ is an initial-value vector contructed from the boundary and normalization conditions at ξ=R. The parameters η_1, η_2 and λ are unknown adjustable initial values. Substitutions of (27b) into (26b) yields a system of six equations

$$(M)\bar{Z}(R) = \begin{Bmatrix} 1 \\ 0 \\ 0 \\ 0 \end{Bmatrix} \tag{28}$$

which must be satisfied at the inner boundary ξ=R.

A solution of the initial-value problem formulated by Eqs. (27) is symbolically denoted by

$$\begin{aligned} \bar{Z}(\xi) &= \bar{Z}(R) + \int_R^{\xi} \bar{H}(\xi,\bar{Z};\eta_1,\eta_2,\lambda;\alpha,\gamma)d\xi \\ &= \bar{Z}(R) + \int_R^{\xi} \bar{H}(\xi,\bar{Z};\bar{\eta};\alpha,\gamma)d\xi \end{aligned} \tag{29}$$

in which

$$\bar{\eta} = \begin{Bmatrix} \eta_1 \\ \eta_2 \\ \lambda \end{Bmatrix}$$

is an unknown vector to be searched. For the given parameters α and γ, values for η_1, η_2 and λ are sought such that the corresponding solution of Eqs. (27) satisfies the three boundary conditions (26c),

$$(N)\bar{Z}(1) = \begin{Bmatrix} 0 \\ 0 \\ 0 \end{Bmatrix} \tag{30}$$

A solution to the eigenvalue problem defined by Eqs. (25) is found when a continuous set of solutions satisfying Eqs. (26) is obtained for the related initial-value problem (27). Thus, for any given values of α and γ,

$$\bar{Y}(\xi) = \bar{Z}(\xi;\bar{\eta}^*;\alpha,\gamma)$$

symbolically denotes a solution to the eigenvalue problem, where

$$\bar{\eta}^* = \begin{Bmatrix} \eta_1^* \\ \eta_2^* \\ \lambda^* \end{Bmatrix}$$

is the root of Eq. (30)

Solving Eq. (30) for the root, $\bar{\eta}^*$, is accomplished by a direct application of Newton's method [12]. Starting with an initial guess $\bar{\eta}^{(0)}$ and given parameters α and λ, the iterative convergent sequence

$$\bar{\eta}^{(k+1)} = \bar{\eta}^{(k)} + \Delta\bar{\eta}^{(k)} \qquad k = 0,1,2,\ldots \tag{31}$$

is generated, where the linear correction at the k-th iteration,

$$\Delta\bar{\eta}^{(k)} = -[(N)(J_1)^{(k)}]^{-1}(N)\bar{Z}(\xi,\bar{\eta}^{(k)},\alpha,\gamma) \quad . \tag{32}$$

is obtained by neglecting higher-order terms of the Taylor's series expansion about $\bar{\eta}^{(k)}$. The Jacobian matrix (J_1) is defined as

$$(J_1)^{(k)} = \left(\frac{\partial \bar{Z}}{\partial \bar{\eta}}\right)^{(k)}_{\xi=1} = \begin{bmatrix} \frac{\partial z_1}{\partial \eta_1} & \frac{\partial z_1}{\partial \eta_2} & \frac{\partial z_1}{\partial \lambda} \\ \frac{\partial z_2}{\partial \eta_1} & \frac{\partial z_2}{\partial \eta_2} & \frac{\partial z_2}{\partial \lambda} \\ \frac{\partial z_3}{\partial \eta_1} & \frac{\partial z_3}{\partial \eta_2} & \frac{\partial z_3}{\partial \lambda} \\ \frac{\partial z_4}{\partial \eta_1} & \frac{\partial z_4}{\partial \eta_2} & \frac{\partial z_4}{\partial \lambda} \\ \frac{\partial z_5}{\partial \eta_1} & \frac{\partial z_5}{\partial \eta_2} & \frac{\partial z_5}{\partial \lambda} \\ \frac{\partial z_6}{\partial \eta_1} & \frac{\partial z_6}{\partial \eta_2} & \frac{\partial z_6}{\partial \lambda} \end{bmatrix}_{\xi=1} \tag{33}$$

and represents a change of final values with respect to a change in the initial $\bar{\eta}$. For constant values of α and γ, the vector

$$\begin{Bmatrix} \Delta\eta_1 \\ \Delta\eta_2 \\ \Delta\lambda \end{Bmatrix} = - \begin{bmatrix} \frac{\partial z_1}{\partial \eta_1} & \frac{\partial z_1}{\partial \eta_2} & \frac{\partial z_1}{\partial \lambda} \\ \frac{\partial z_2}{\partial \eta_1} & \frac{\partial z_2}{\partial \eta_2} & \frac{\partial z_2}{\partial \lambda} \\ \frac{\partial z_6}{\partial \eta_1} - \nu \frac{\partial z_5}{\partial \eta_1} & \frac{\partial z_6}{\partial \eta_2} - \nu \frac{\partial z_5}{\partial \eta_2} & \frac{\partial z_6}{\partial \lambda} - \nu \frac{\partial z_5}{\partial \lambda} \end{bmatrix}^{-1}_{\xi=1} \begin{Bmatrix} z_1 \\ z_2 \\ z_6 - \nu z_5 \end{Bmatrix}_{\xi=1} \tag{34}$$

provides the linear correction of the estimated data η_1, η_2 and λ. If the initial estimate of $\bar{\eta}$ is chosen in a sufficiently small neighborhood of the root $\bar{\eta}^*$, the sequence (31) will converge to the root $\bar{\eta}^*$ of Eq. (30). Due to the nonlinearity of the vector function $\bar{H}$, an explicit solution of the initial-value problem (27) cannot be readily obtained and therefore the expression for the Jacobian (J_1) cannot be determined directly. Thus, a method for constructing (J_1) for any given iteration step is necessary. Differentiation of the initial-value problem with respect to $\bar{\eta}$ results in the variational equations

$$\frac{d}{d\xi}\left\{\frac{\partial \bar{Z}}{\partial \eta_1}\right\} = \left(\frac{\partial \bar{H}}{\partial \bar{Z}}\right)\left\{\frac{\partial \bar{Z}}{\partial \eta_1}\right\} \tag{35a}$$

$$\left\{\frac{\partial \bar{Z}}{\partial \eta_1}\right\}_{\xi=R} = \begin{Bmatrix} 0 \\ 0 \\ 1 \\ -\frac{1}{R} \\ 0 \\ 0 \end{Bmatrix} \tag{35b}$$

$$\frac{d}{d\xi}\left\{\frac{\partial \bar{Z}}{\partial \eta_2}\right\} = \left(\frac{\partial \bar{H}}{\partial \bar{Z}}\right)\left\{\frac{\partial \bar{Z}}{\partial \eta_2}\right\} \tag{35c}$$

$$\left\{\frac{\partial \bar{Z}}{\partial \eta_2}\right\}_{\xi=R} = \begin{Bmatrix} 0 \\ 0 \\ 0 \\ 0 \\ 1 \\ \frac{\nu}{R} \end{Bmatrix} \tag{35d}$$

$$\frac{d}{d\xi}\left\{\frac{\partial \bar{Z}}{\partial \lambda}\right\} = \left(\frac{\partial \bar{H}}{\partial \bar{Z}}\right)\left\{\frac{\partial \bar{Z}}{\partial \lambda}\right\} + \left\{\frac{\partial \bar{H}}{\partial \lambda}\right\} \tag{35e}$$

$$\left\{\frac{\partial \bar{Z}}{\partial \lambda}\right\}_{\xi=R} = \begin{Bmatrix} 0 \\ 0 \\ 0 \\ \frac{R}{2}\gamma \\ 0 \\ 0 \end{Bmatrix} . \tag{35f}$$

Equations (35b), (35d) and (35f) provide the initial conditions for the variational problem. The eighteen first-order equations which result from performing the operations indicated by Eqs. (35a), (35c) and (35e) are listed in Appendix B. For given values of α and γ, and a given vector $\bar{\eta}$, the initial-value problem (27) may be integrated numerically with a Runge-Kutta method. Evaluation of the resulting solution to the variational problem at $\xi=1$ provides the Jacobian matrix (J_1) which corresponds to selected values of $\bar{\eta}$, α and γ. Setting $\bar{\eta} = \bar{\eta}^{(0)}$ and integrating Eqs. (27) and (35) over the interval from $\xi=R$ to $\xi=1$ yields a corrected vector $\bar{\eta}^{(1)}$, which is calculated from Eqs. (34). Repeating the same operations with $\bar{\eta} = \bar{\eta}^{(1)}$, a second corrected vector $\bar{\eta}^{(2)}$ is obtained. Repetition of this procedure results in convergence to the desired solution $\bar{\eta}^*$, a root of Eq. (30). Having obtained a root $\bar{\eta}^{(j)}$ for a given $\alpha = \alpha^{(j)}$ and γ, the value of α may be perturbed,

$$\alpha = \alpha^{(j+1)} = \alpha^{(j)} + \Delta\alpha^{(j)} \qquad j = 0,1,2,\ldots,m$$

For this new α, iteration is restarted from the previously obtained values of $\bar{\eta} = \bar{\eta}^{(j)}$. For sufficiently small values of $\Delta\alpha^{(j)}$, $\bar{\eta}^{(j)}$ is within the new contraction domain of Newton's method, and the iteration will converge to the new root $\bar{\eta}^{(j+1)}$, corresponding to the new $\alpha = \alpha^{(j+1)}$. The range of α is limited by the finite amplitudes of vibration for which the Eqs. (25) were derived.

Thus, by integrating the initial-value problems (27) and (35) with a Runge-Kutta technique, and performing successive corrections by Newton's method, approximate numerical solutions may be obtained for the nonlinear eigenvalue problem defined by Eqs. (25).

The numerical computation procedure used in the investigation of the nonlinear free vibration characteristics of the plate-mass system is given as follows.

Initially, the linear free vibration problem is considered; accordingly, the amplitude parameter α is first set equal to zero. Then, the initial-value problem (27) can be integrated numerically with the estimated initial values $\bar{\eta}^{(0)}$. Using Newton's method, successive corrections of η_1, η_2, and λ were performed until the final values, $\bar{Z}(1)$, satisfied the inequality,

$$\max_{1\leq i\leq 3} \left| \sum_{j=1}^{6} n_{ij} Z_j(1) \right| \leq 0.1 \times 10^{-5}$$

where $(n_{ij}) = (N)$, and the prescribed error is consistent with the fourth order Runge-Kutta method using a step size of $\Delta\mu = \frac{1}{40}$ on the interval [R,1]. The solution for the linear free vibration of the system is obtained and the corresponding values of $\bar{\eta}^* = (\eta_1^*, \eta_2^*, \lambda^*)^T$ are stored. The resonance curves are obtained by successively incrementing the amplitude parameter α and initiating iteration for each increment with the previously obtained values of the root $\bar{\eta}$.

RESULTS OF NUMERICAL COMPUTATIONS

To provide a check on the method of solution, the plate-mass system may be reduced to model a flat circular plate by equating the mass ratio to unity, and assigning a relatively small value to the radius ratio. Since the mass ratio, γ, is defined as the ratio of the mass of the central rigid part to the mass of the plate it replaces, $\gamma=1$ describes a plate-mass system of the same mass as a flat circular plate. The stiffness of a flat circular plate can be approximated by selecting a small radius ratio. For the rigid core under consideration, the continuity and symmetry conditions of zero slope and radial deflection at the center of a flat circular plate are also approached as the radius ratio tends to zero. Accordingly, $R=0.025$ was selected since it also falls on a radius defined by a convenient step size in the numerical integration. The harmonic response curve thus obtained is presented by the smooth curve in Fig. 2, where W_R is the deflection at the inner boundary, and ω is the dimensionless angular frequency. Sandman and Huang [7,13], also employed von Karman's equation in the determination of the nonlinear resonance curve for flat circular plates, while Chiang and Chen [4] solved the Berger equations and reduced the plate-mass problem to that of a flat plate. Values found by Sandman and Huang are shown as small circles in Fig. 2, and the close agreement supports the results of the present investigation for nonlinear free vibrations. Values taken from the curves found by Chiang and Chen are indicated by the small squares also in Fig. 2. The greater nonlinear frequencies exhibited by their curve is consistent with the observation of Ramachandran [6], that Berger's equations give higher values for the nonlinear frequency.

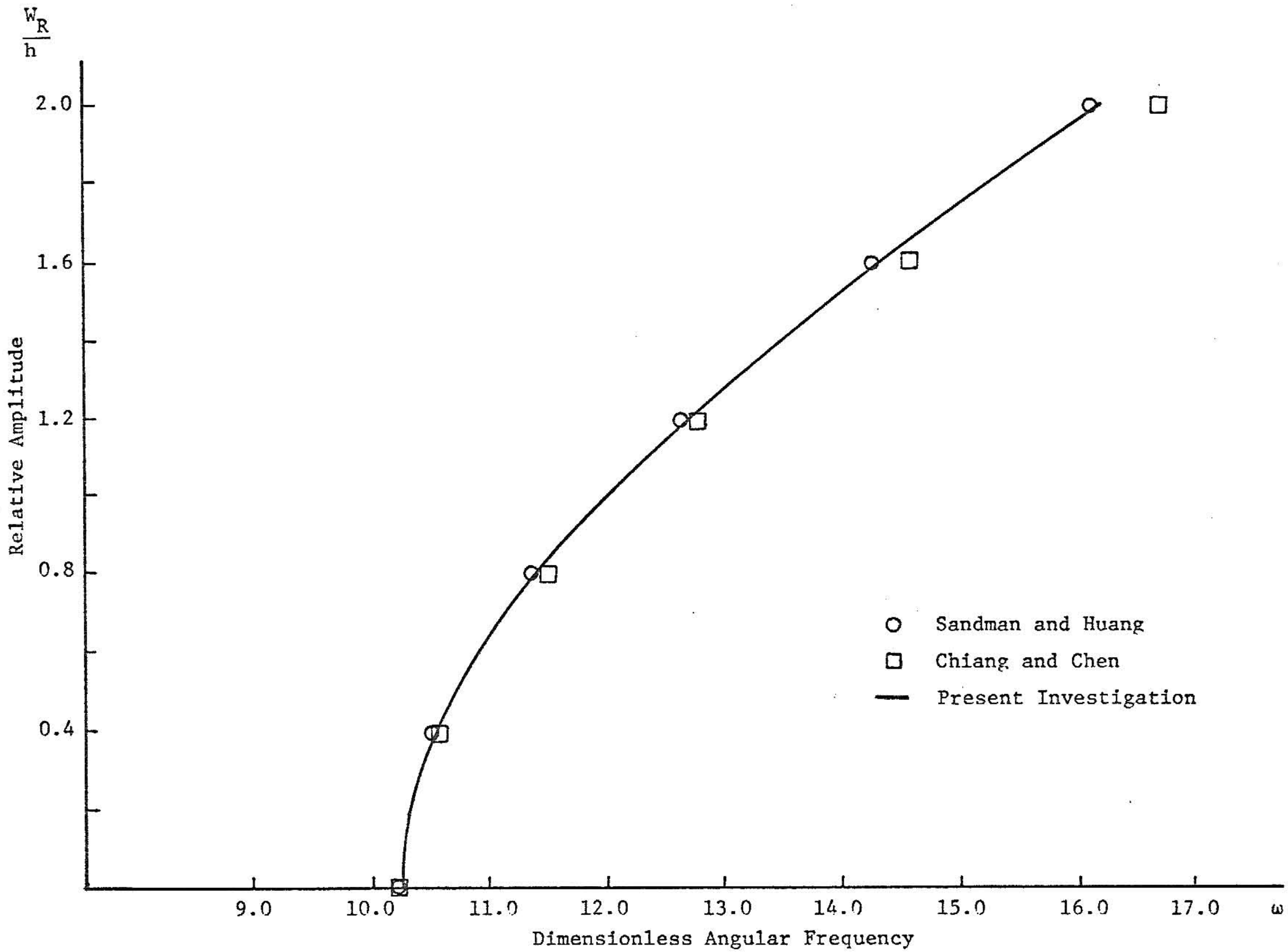

Fig. 2. Harmonic response of a clamped circular plate.

In that the linear vibration characteristics are found to be useful in an explanation of the nonlinear behavior of the plate-mass system, the nonlinear problem formulated was reduced accordingly by prescribing $\alpha=0$. and then solving the resulting linear problem for various mass and radii ratios. Figure 3 presents the non-dimensional linear frequencies thus obtained as a function of the radius ratio R. Since the linear problem has been studied by other authors, the determination of the natural frequencies offered an additional check on the method of solution employed in this investigation. Handelman and Cohen, [3], presented a set of approximate curves similar to those of Fig. 3. Several more precisely determined values were also given for mass ratios of 2.0 and 10.0. Those values are shown as small circles in Fig. 3 and the excellent agreement is quite apparent.

A numerical comparison with values obtained by Chiang and Chen [4] is offered in Table 1, and the values found for the linear frequency parameters agree well for radii ratios of 0.1 and 0.3. The differences noted between the two flat circular plate models are recognized to be consistent with the different radii ratios employed.

If a point mass is added to a flat circular plate, the frequency of the plate-mass system will be lower than that of the original plate. However, when a rigidly attached mass occupying a finite area is added to the system, the effect on the frequency is not completely obvious. This phenomenon occurs because adding a rigid mass produces a change in the kinetic energy which must compete with a change in the potential energy due to the stiffening effect introduced at the plate-mass boundary. Hence, the plate behavior is dependent upon the specific mass and radius ratios in the system under consideration.

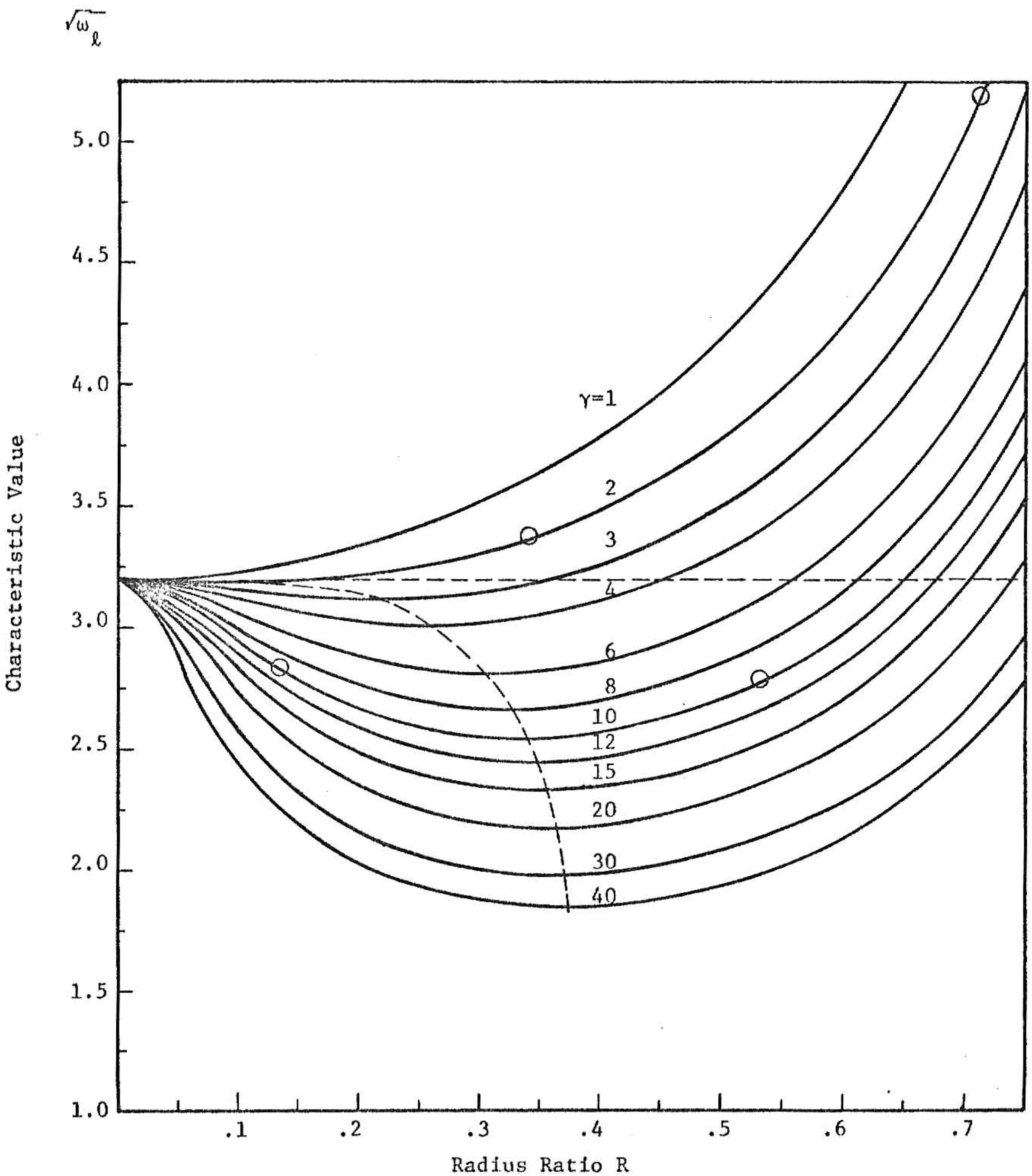

Fig. 3. Linear resonant frequencies of plate-mass systems.

TABLE 1

Characteristic Value $\sqrt{\omega_\ell}$ for Linear Free Vibrations

R / γ	0.025	0.001	0.1		0.3	
	Present Investigation	Chaing and Chen	Present Investigation	Chaing and Chen	Present Investigation	Chaing and Chen
1.0	3.1995	3.1962	3.2313	3.2311	3.5914	3.5913
2.0	3.1968	3.1962	3.1937	3.1935	3.3066	3.3065
8.0	3.1809	3.1962	3.0014	3.0012	2.6714	2.6714
16.0	3.1602	3.1962	2.8097	2.8095	2.3161	2.3160

The general behavior of the curves in Fig. 3 is explainable through arguments based on the fundamentals of vibratory systems. It is first obvious that as long as the mass ratio is less than or equal to unity, the stiffening produced by imposing a rigid core of any radius on the plate will always increase the natural frequency of the plate. For a mass ratio less than unity, increasing the radius ratio actually subtracts mass from the system while simultaneously increasing the stiffness. Hence, the frequency will increase. A mass ratio of unity defines a system with a total mass equal to that of a flat circular plate. Therefore, increasing the radius ratio only increases the rigidity of the plate and the frequency would also increase.

For mass ratios slightly greater than unity, the behavior must be examined more carefully. Figure 4 presents a more refined view of Fig. 3 for small values of the parameters γ and R. Given a mass ratio greater than unity, increasing the radius ratio simultaneously increases the total mass of the system. Since an increase in the radius of the rigid core also increases the stiffness, the introduction of the rigid mass has two opposing effects on the frequency, where as the effects were complimentary for mass ratios less than unity. Handelman & Cohen, [3], found that if the mass ratio is less than 1.8, the frequency will always increase if the radius ratio is increased. Thus, for constant mass ratios less than the critical γ_c=1.8, the increased stiffness accompanying an increase in the radius always increases the frequency despite the related addition of mass. Referring to Fig. 4, it is noted that the frequency will always be higher than that of a flat circular plate for mass ratios less than this critical value.

Considering mass ratios greater than the critical value, the frequency initially decreases as the radius ratio increases from zero, and the effect

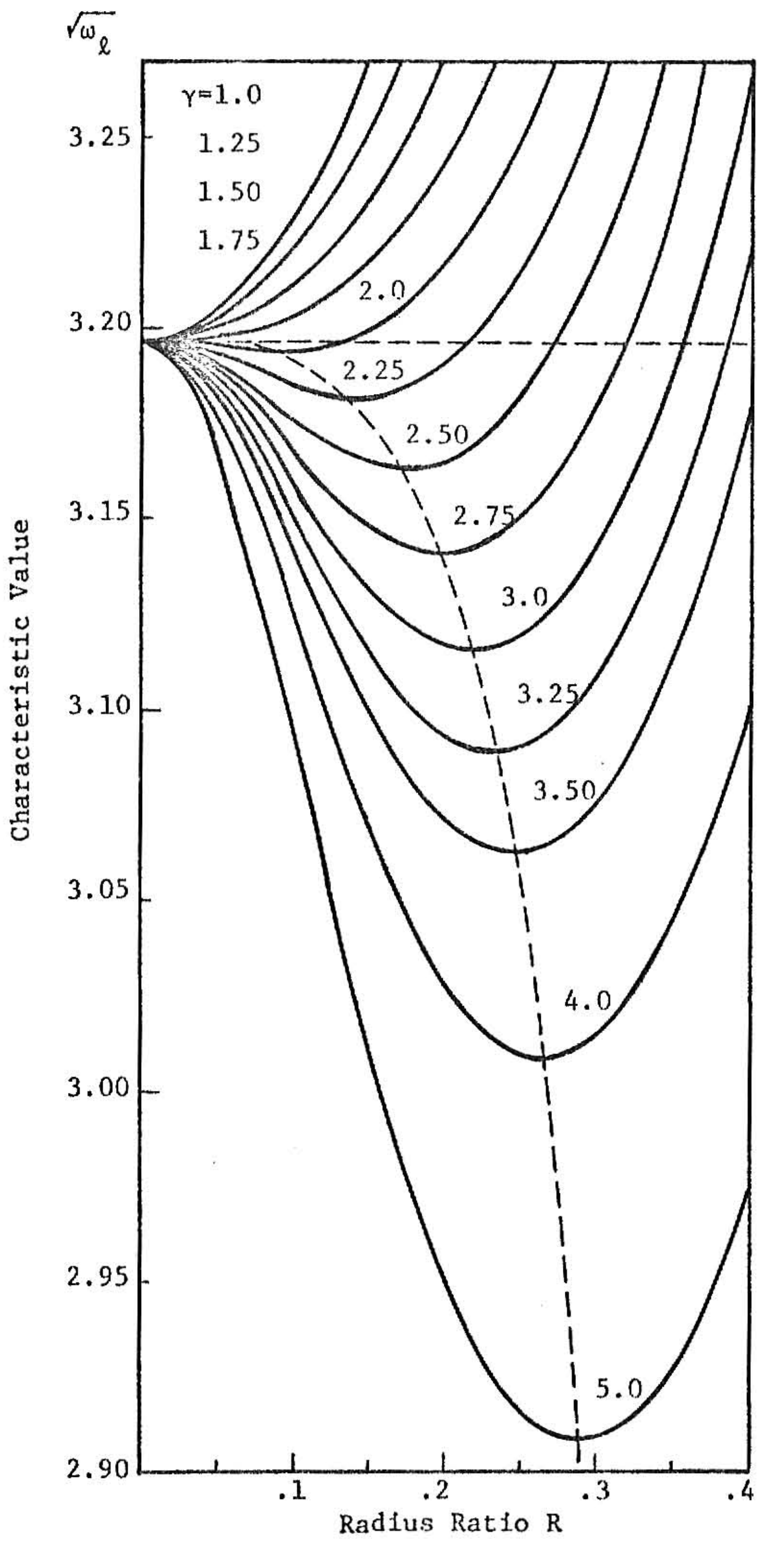

Fig. 4. Linear resonant frequencies of plate-mass systems.

of the added mass is seen to influence the frequency more than the increase in stiffness. As the radius ratio is further increased, a transition point is reached where the influence of the increasing stiffness overtakes that of the accompanying increase in mass. Referring to Figures 3 and 4, the dashed curves drawn through the points of lowest frequency for constant mass ratios defines these transition points. Increases in radii ratios beyond these points produces increases in the linear frequency of the plate-mass system. Curve A of Fig. 5 defines the corresponding values of mass and radii ratios at which the transition occurs. It will be later apparent that the values of the γ and R parameters in relation to the transition points similarly affects the behavior at large amplitudes.

When considering the linear problem, an additional point of interest is discovered when the radius ratio is increased beyond the transition point until the frequency of the plate-mass system equals that of a flat circular plate. The horizontal dashed line in Figures 3 and 4 locates these cross-over points, and the corresponding curve B in Fig. 5 allows determination of the unique mass and radii ratios for which the cross-over occurs. This curve was found to be in excellent agreement with one presented by Handelman and Cohen [3].

Since the primary intention of this research was to determine the non-linear behavior of plate-mass systems, a direct analytical method of determining the transition points of Fig. 5 was not attempted. Rather, the curve was constructed through visual identification of the parameter values at points of horizontal tangency. An analytical minimization should provide the means to determine more precisely the points of transition, since, as previously suggested, this linear phenomenon may also be of importance in predicting and interpreting the nonlinear behavior.

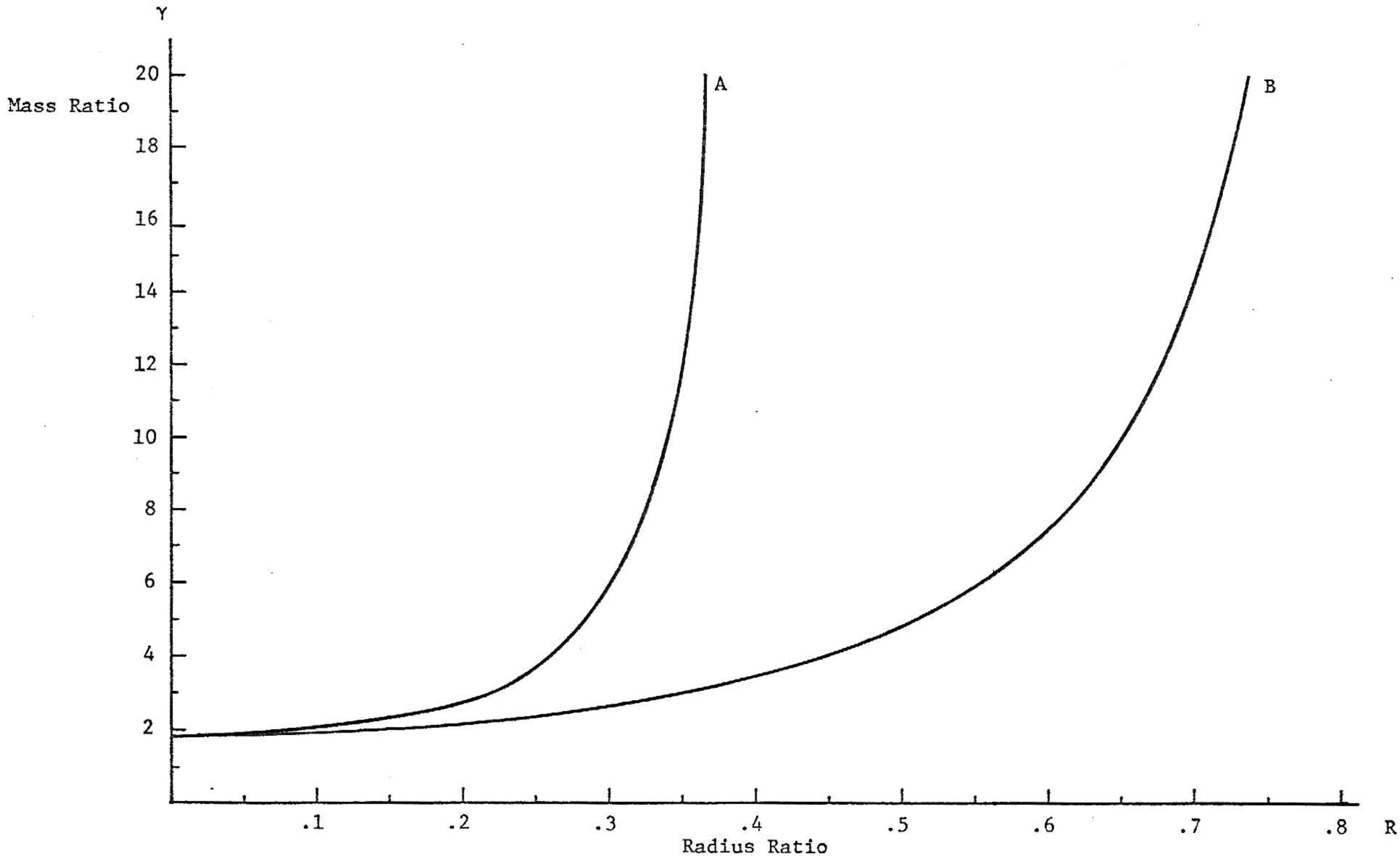

Fig. 5. Mass and radius ratios at transition and cross-over.

Extending the problem beyond linear considerations, Figs. 6-10 are plotted from the numerically obtained results for nonlinear vibrations. Selected values from the computed data used to plot the resonance curves are given in Tables 2-6. The figures are presented with the non-dimensional amplitudes, W_R/h, plotted as a function of the dimensionless angular frequency parameter, $\omega-\omega_\ell$, where ω and ω_ℓ are respectively the nonlinear and linear resonant frequencies. Resonance curves are given for plate-mass systems with constant radii ratios so that plotting the mass ratio as a variable parameter shows the effect of adding mass to the vibrating system. In each case considered, the addition of mass reduces the hard-spring behavior and tends to linearize the vibratory nature of the system. The increased shear force on the plate inner boundary resulting from an increase in the mass, and hence in the related D'Alembert force, is seen to induce equivalent amplitudes of vibration with smaller increases beyond the linear frequency. A reference to Eqs. (25) substantiates the noted effects of mass addition.

While Table 1 emphasizes the close agreement obtained in linear frequencies whether utilizing Berger's simplified equations or the more rigorous von Karman approach, Fig. 2 demonstrates a divergence of the frequency predictions when nonlinear vibrations are considered. Although the disagreement is not large, it should be noted that the frequencies compared are those of a flat circular plate, and as suggested by Nowinski and Ohnabe [5], altering the boundary conditions to those inherent in the present investigation could lead to even greater discrepencies. An indication of the magnitude of disagreement found between the Berger and von Karman approaches is provided in Figs. 11 and 12. Values taken from the curves given by Chiang and Chen [4] are compared to frequencies predicted with the von Karman equations employed in this investigation. The differences are seen to be quite significant and

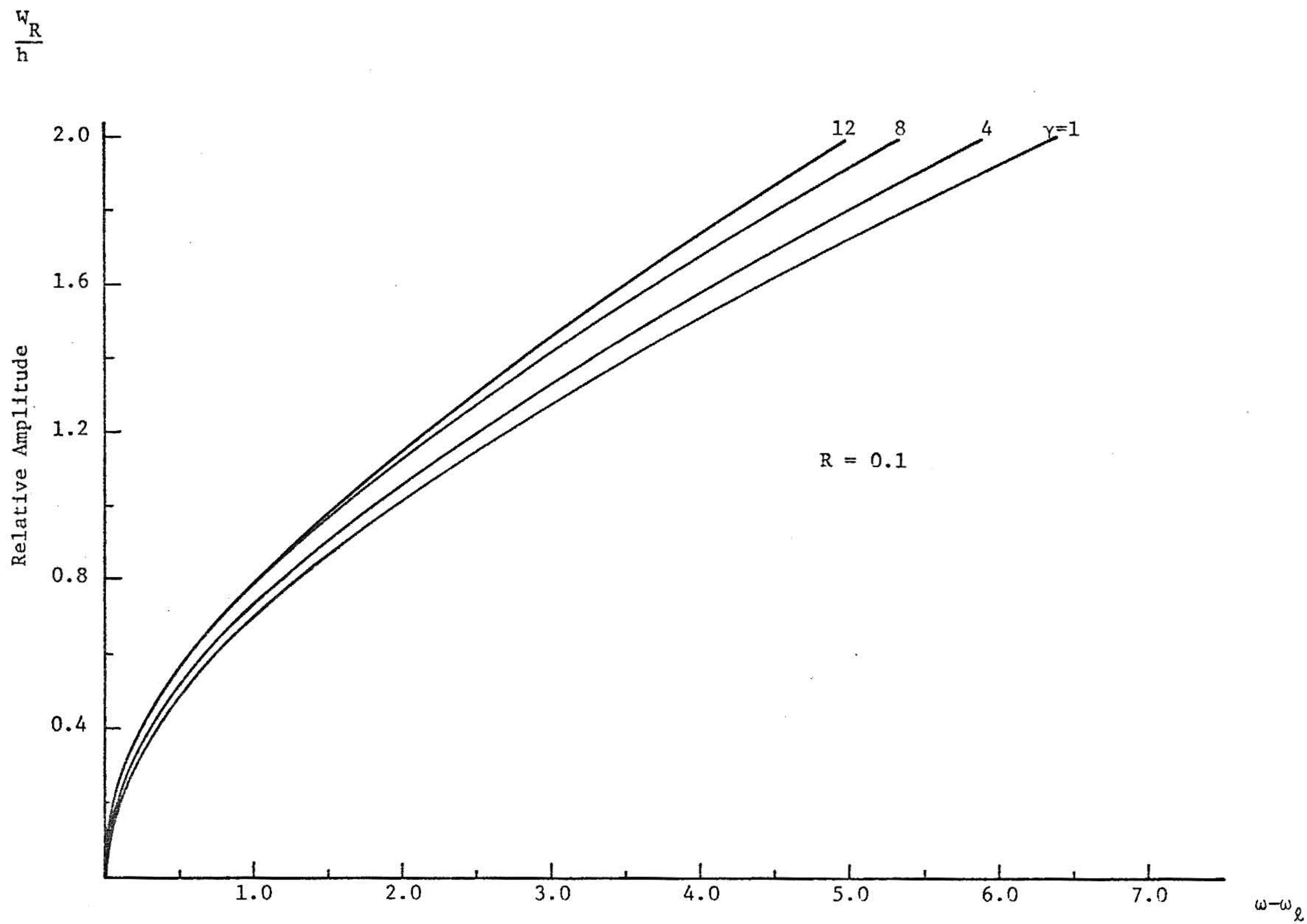

Fig. 6. Harmonic response of plate-mass systems with R = 0.1.

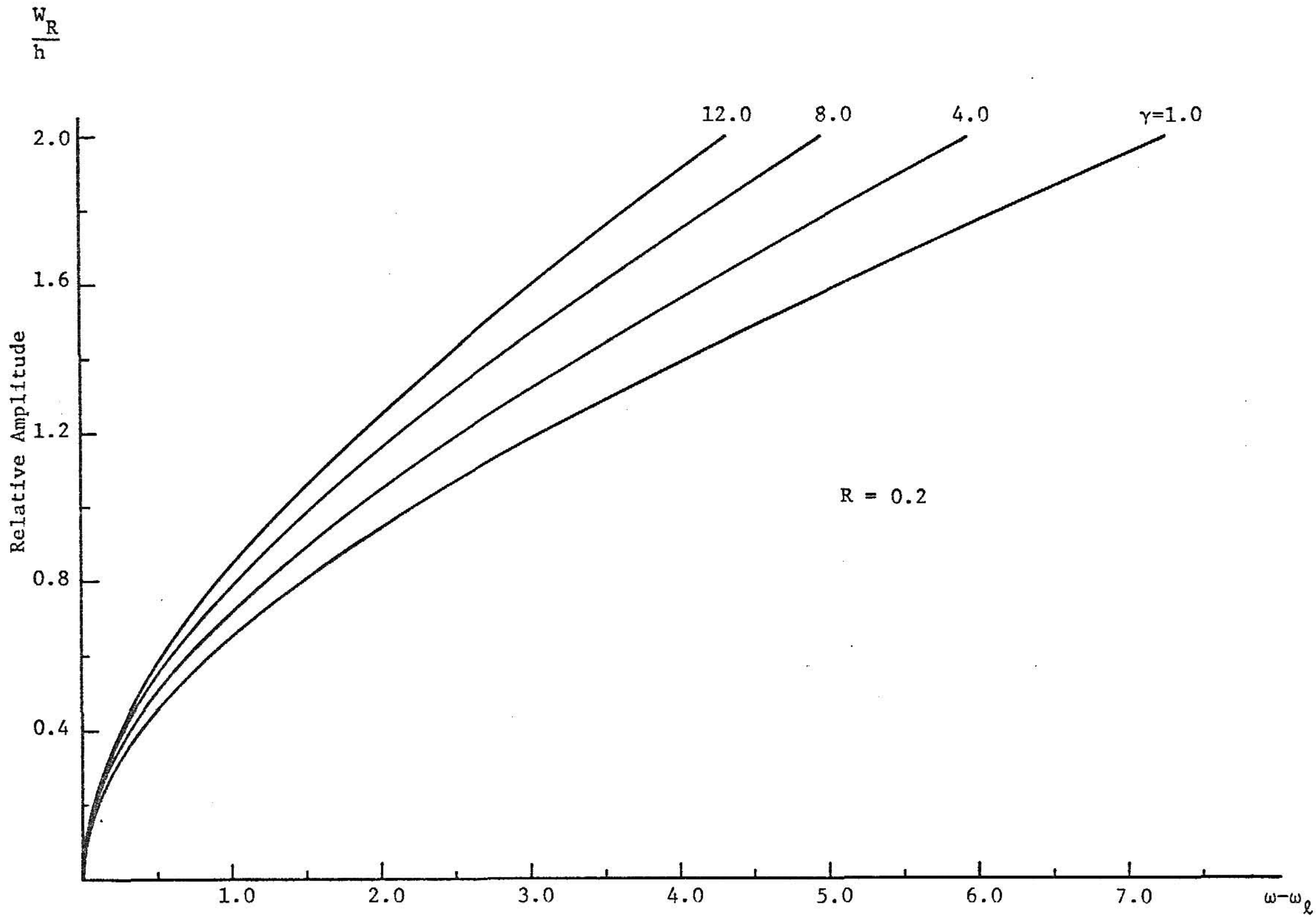

Fig. 7. Harmonic response of plate-mass systems with R = 0.2.

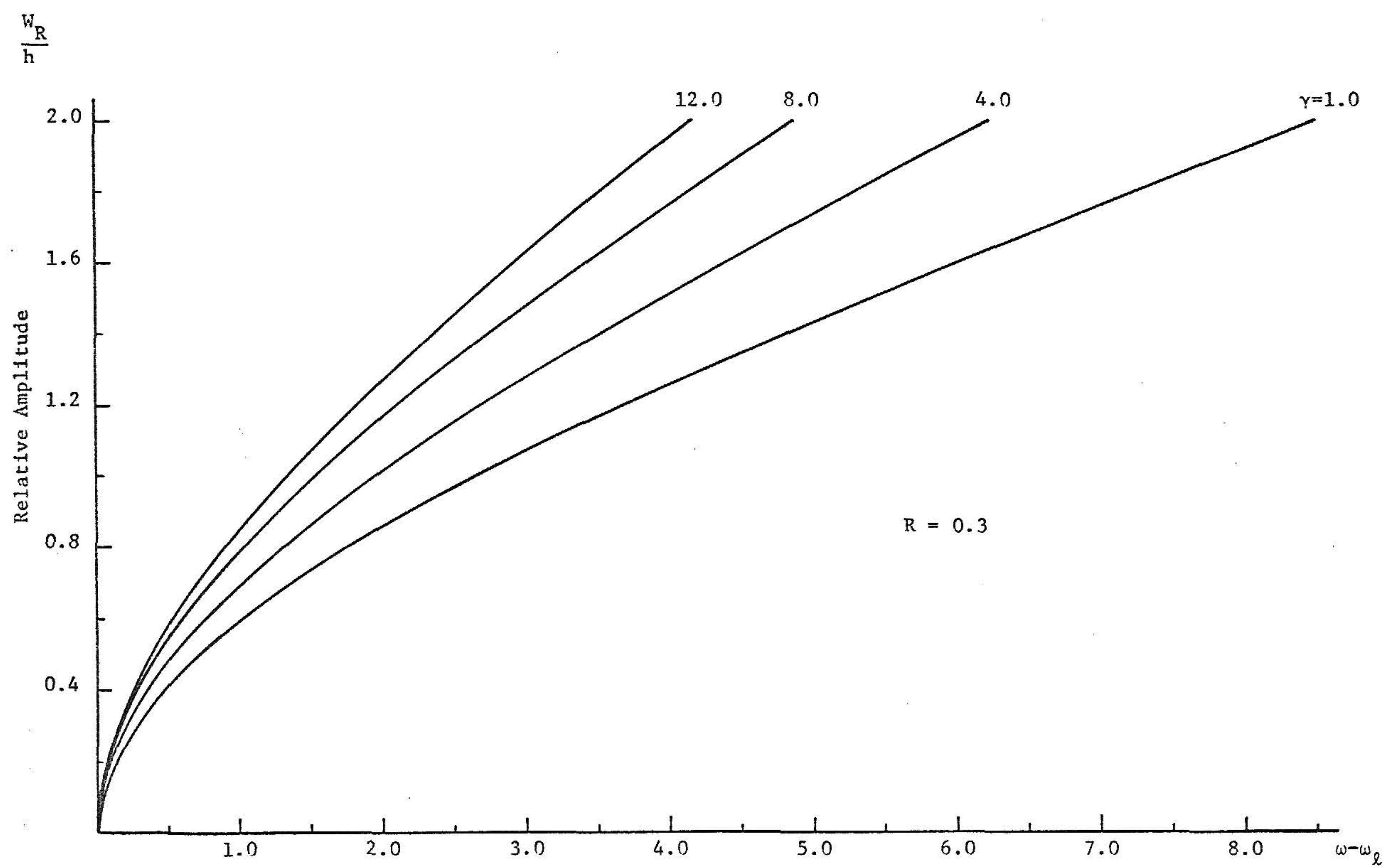

Fig. 8. Harmonic response of plate-mass systems with R = 0.3.

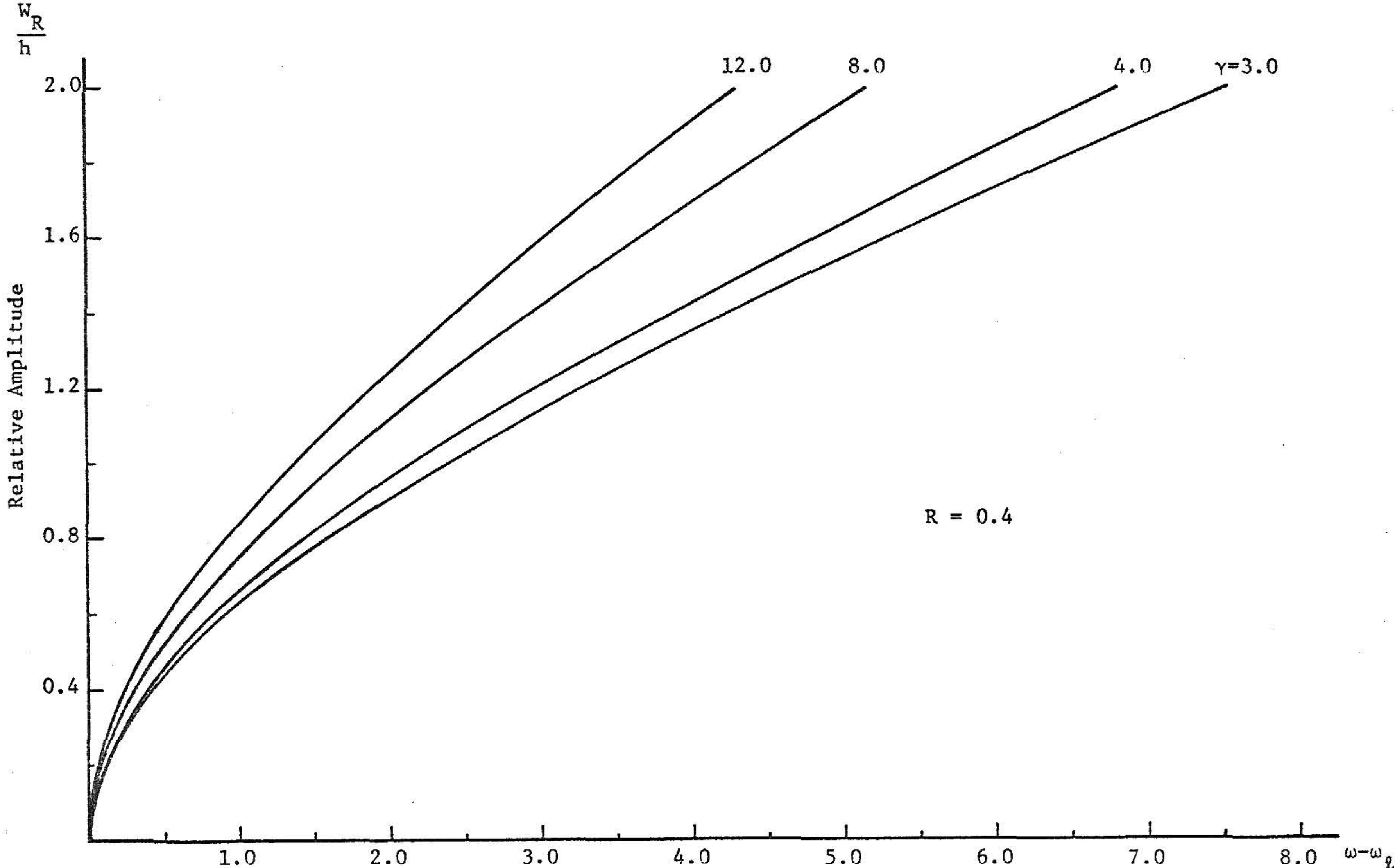

Fig. 9. Harmonic response of plate-mass systems with R = 0.4.

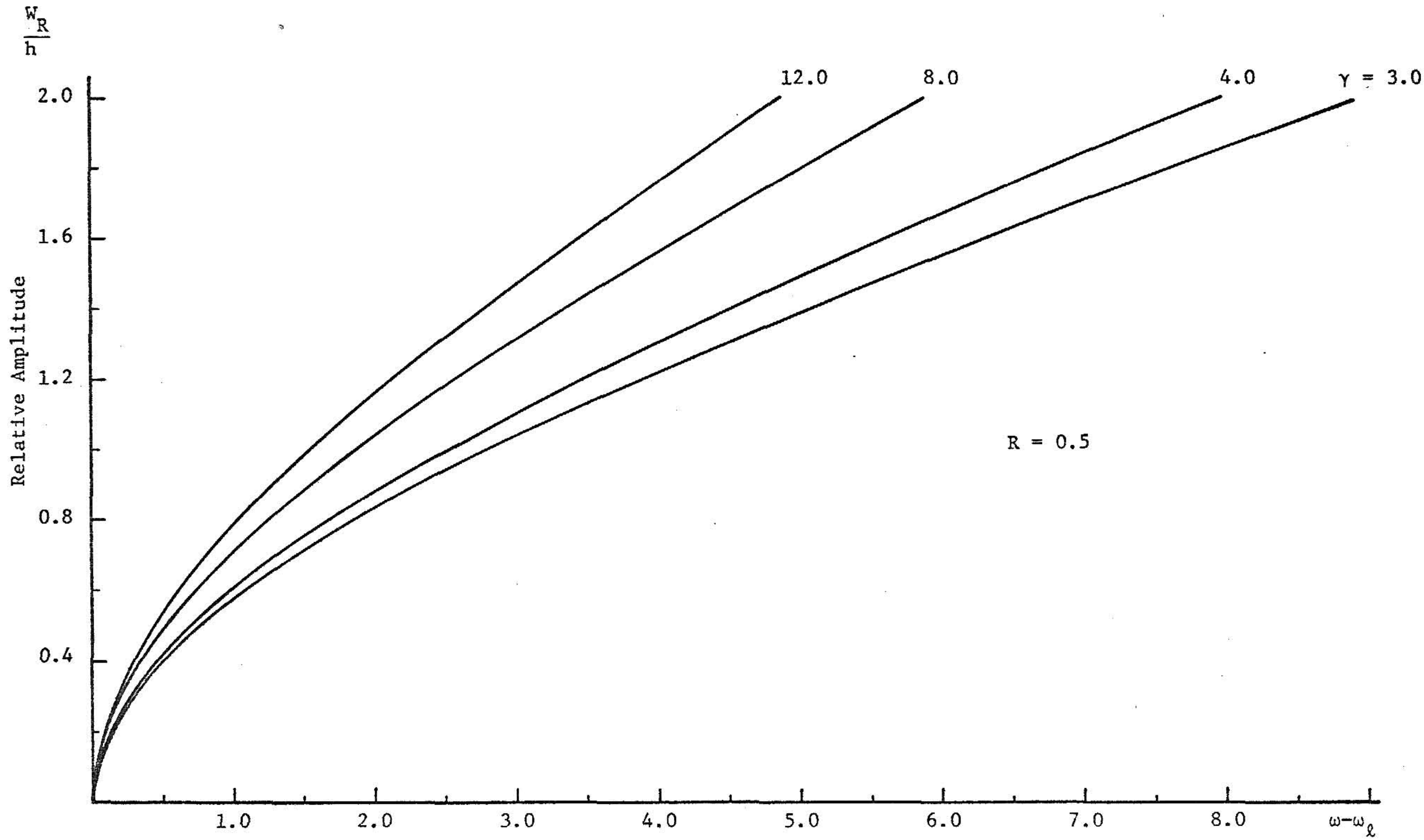

Fig. 10. Harmonic response of plate-mass systems with R = 0.5.

TABLE 2

Dimensionless Angular Frequency, ω

$\gamma = 1.0$				
W_R/h \ R	0.025	0.1	0.2	0.3
0	10.2367	10.4410	11.1341	12.3858
0.4	10.5430	10.7784	11.5291	12.8549
0.8	11.4103	11.7265	12.6303	14.1565
1.2	12.7203	13.1425	14.2547	16.0621
1.6	14.3501	14.8841	16.2269	18.3574

TABLE 3

Dimensionless Angular Frequency, ω

$\gamma = 3.0$					
W_R/h \ R	0.1	0.2	0.3	0.4	0.5
0	9.9718	9.7138	9.8871	10.6718	12.3112
0.4	10.2941	10.0060	10.2630	11.0948	12.8121
0.8	11.1987	11.0229	11.3051	12.2641	14.1948
1.2	12.5466	12.4399	12.8277	13.9661	16.2022
1.6	14.1986	14.1531	14.6558	16.0014	18.5971

TABLE 4

Dimensionless Angular Frequency, ω

$\gamma = 4.0$					
W_R/h \ R	0.1	0.2	0.3	0.4	0.5
0	9.7571	9.1738	9.0898	9.6336	10.9737
0.4	10.0724	9.5008	9.4355	10.0153	11.4201
0.8	10.9571	10.4108	10.3936	11.0707	12.6521
1.2	12.2740	11.7485	11.7931	12.6063	14.4404
1.6	13.8859	13.3640	13.4722	14.4420	16.5733

TABLE 5

Dimensionless Angular Frequency, ω

$\gamma = 8.0$					
W_R/h \ R	0.1	0.2	0.3	0.4	0.5
0	9.0084	7.6526	7.1365	7.2987	8.1282
0.4	9.2992	7.9254	7.4078	7.5877	8.4586
0.8	10.1143	8.6843	8.1596	8.3866	9.3703
1.2	11.3241	9.7982	9.2569	9.5484	10.6932
1.6	12.7993	11.1405	10.5719	10.9364	12.2703

TABLE 6

Dimensionless Angular Frequency, ω

$\gamma = 12.0$					
W_R/h \ R	0.1	0.2	0.3	0.4	0.5
0	8.3995	6.6946	6.0645	6.1109	6.7464
0.4	8.6703	6.9331	6.2950	6.3528	7.0205
0.8	9.4287	7.5965	6.9335	7.0213	7.7769
1.2	10.5525	8.5696	7.8651	7.9934	8.8743
1.6	11.9196	9.7411	8.9811	9.1544	10.1824

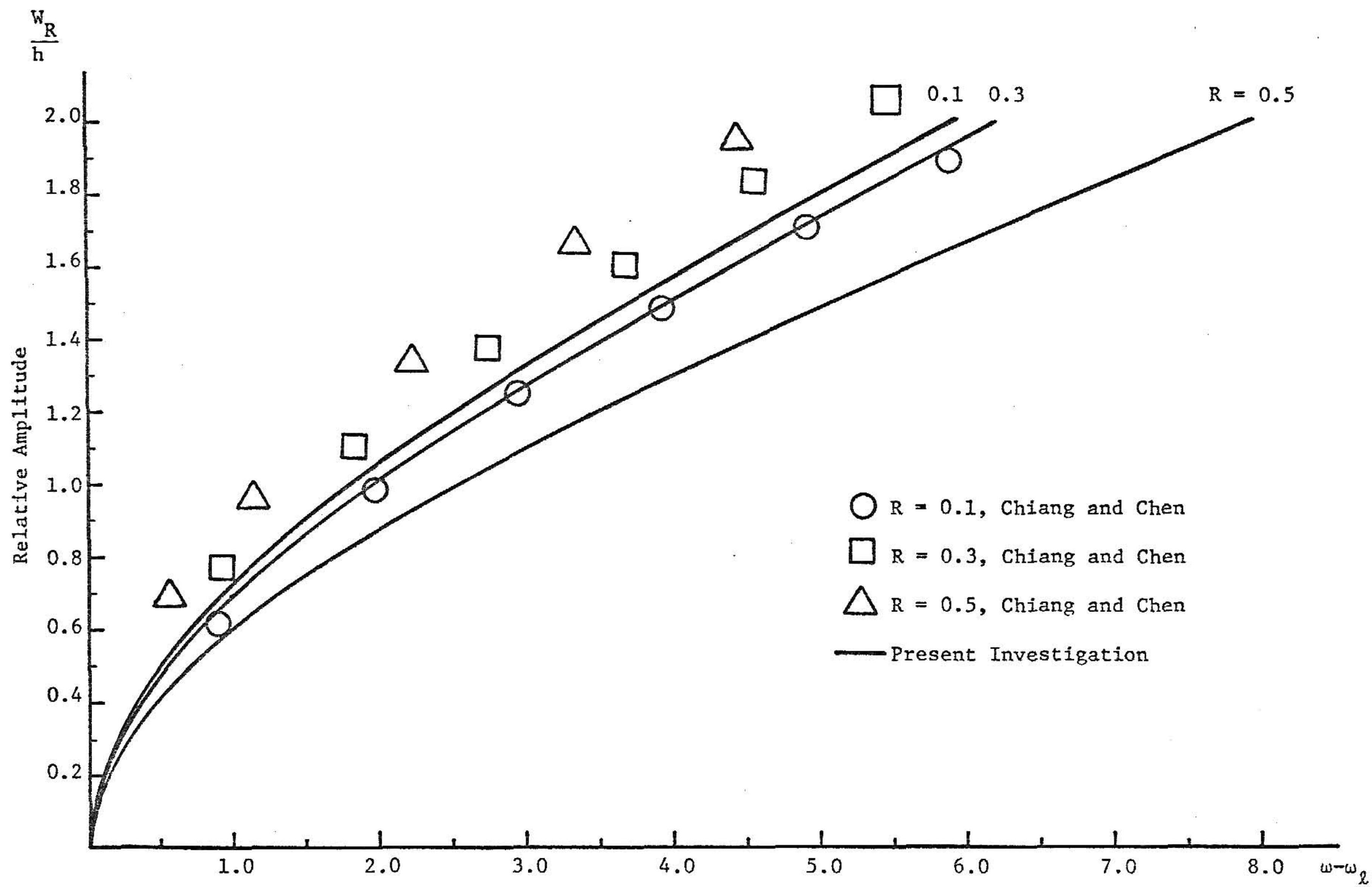

Fig. 11. Harmonic response of plate-mass systems with γ = 4.0.

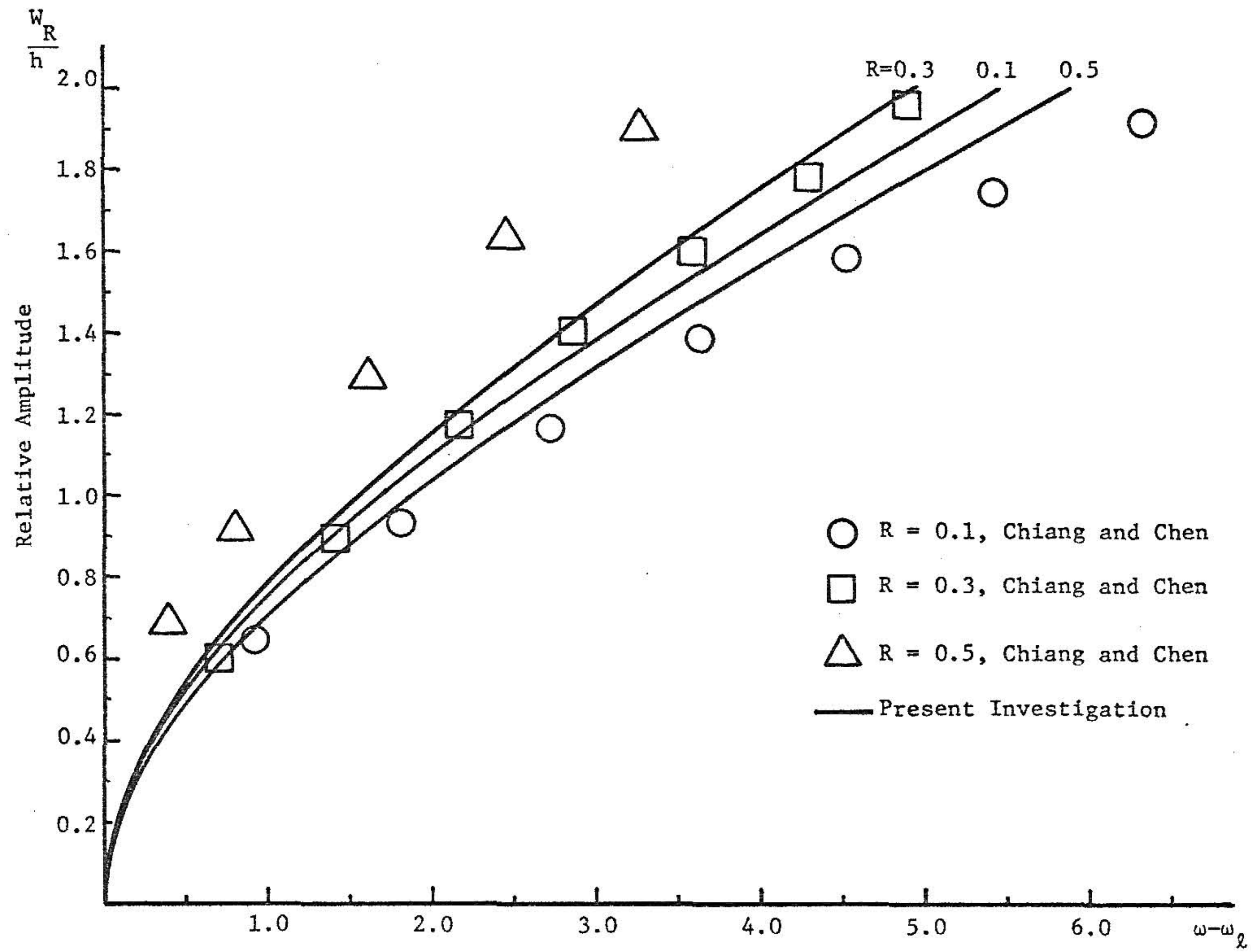

Fig. 12. Harmonic response of plate-mass systems with γ = 8.0.

they may be attributed to several factors. Intuitively, the more rigorous von Karman equations should provide more accurate results than the simplified Berger-type equations. However, the contributions of the terms of the second invariant of the membrane strain may actually be of secondary importance when considering discrepencies of the magnitude noted in this investigation. The errors associated with using various boundary conditions in conjunction with Berger's simplification were studied by Nowinski and Ohnabe, and such contributions to the differing nonlinear frequencies may be significant. Notably, they discovered that the accuracy of the Berger method is closely associated with the restrictions placed on the in-plane displacements of the edges of the plate. Thus, the inclusion of a concentric rigid mass introduces still another opportunity for the solution to go astray. The plate stiffness and related memberane stresses associated with a large R may introduce larger errors of this nature than those occurring with a smaller radius ratio since the increased stiffness in the former case places increased emphasis upon boundary conditions. The closer agreement of the two methods at small radii ratios is notably consistant with this observation.

The curves in Figs. 11 and 12 are given for constant mass ratios and thus provide an alternate study of the change in nonlinear behavior resulting from a change in the radius ratio. From the relation, $\gamma = M/\pi b^2 \rho h$, it is obvious that at a constant mass ratio, changing the radius of the rigid core introduces a corresponding change in the mass M proportional to b^2. Hence, changing the parameter R simultaneously changes both the mass and the stiffness of the vibratory system. As evidenced by Eqs. (25), such changes could be expected to alter the nonlinear behavior as well as the linear frequency. Limiting comments to the present investigation and remembering that amplitudes are given at differing radii, Fig. 11 demonstrates that an increase in the radius ratio bends the response curve to the right. However, at the different mass ratio presented in Fig. 12, increasing the radius ratio initially bends the response curve to the left before imitating the effects found in Fig. 11. Although the changes in nonlinearity appear to be governed by the transition points similar to those given in Figs. 3, 4 and 5, the present numerical investigation was not sufficiently exhaustive to determine the exact nature of the phenomenon.

EXPERIMENTAL INVESTIGATION

In order to provide further verification of the nonlinear resonance curves obtained by the numerical method, an experimental study was conducted to determine the amplitude-frequency relationship for the first mode of vibration of two different plate-mass models. The following text presents a description of the equipment used, the procedure followed and the results obtained.

Experimental Apparatus and Instrumentation

Figure 13 pictures the two flat circular plates, their respective concentric rigid masses, and the plate clamping fixture used. The plates were fabricated from 20 ga. sheet metal, and the rigid center clamps were machined from a steel shaft.

Cross-sectional views of the two rigid centers are shown twice the actual size in Figures 14 and 15. Each center clamp was designed to approach the theoretical boundary conditions of zero slope and radial deflection at the clamped inner boundary of the circular plates. In order to uniformly clamp the inner radius, a 0.001 inch taper was machined on the clamping surfaces of the rigid mass shown in Fig. 15. A 1/2-inch high strength bolt provided the means to rigidly clamp the identical halves to each side of the plate. The cylindrical shell design, shown in Fig. 14, was fabricated to provide a lower mass ratio while simultaneously satisfying the appropriate boundary conditions. A 3/8-inch socket head cap screw fastened the mating halves to the plate. The dimensions and physical properties of the two test specimens are given in Table 7.

At the outer radius, the plate was clamped between the two ten inch pipe flanges also shown in Fig. 13. With the rigid mass attached, the

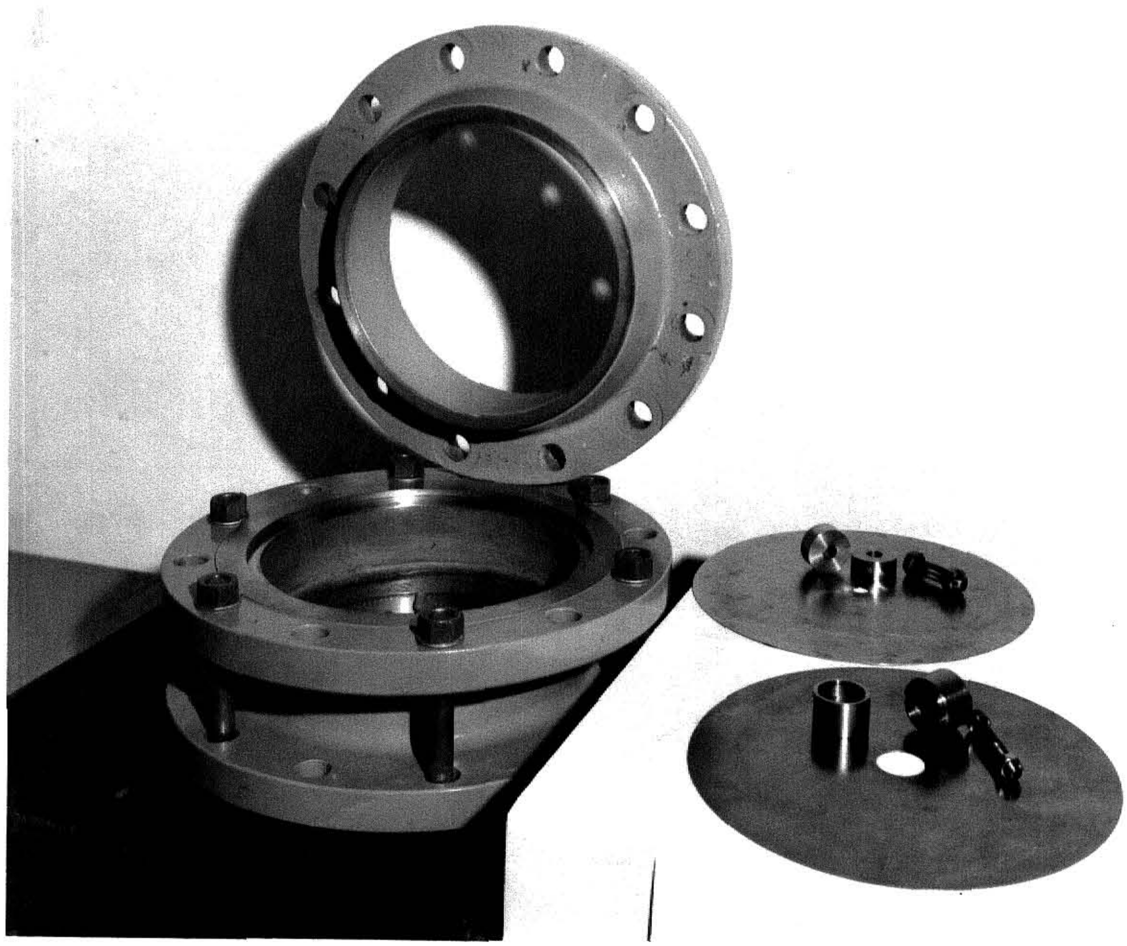

Fig. 13. Test Specimens and Plate Clamping Fixture.

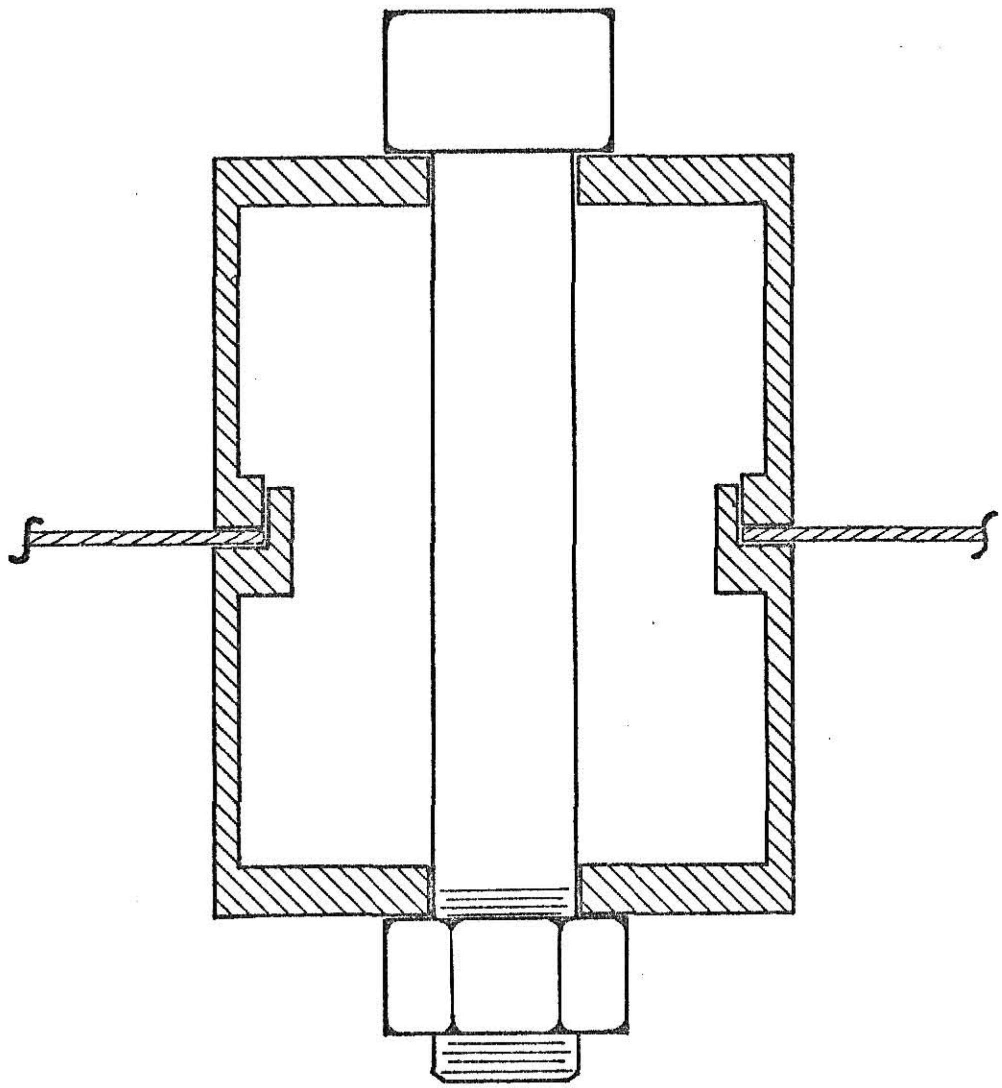

Fig. 14. Rigid Mass of Cylindrical Shell Design, Specimen A.

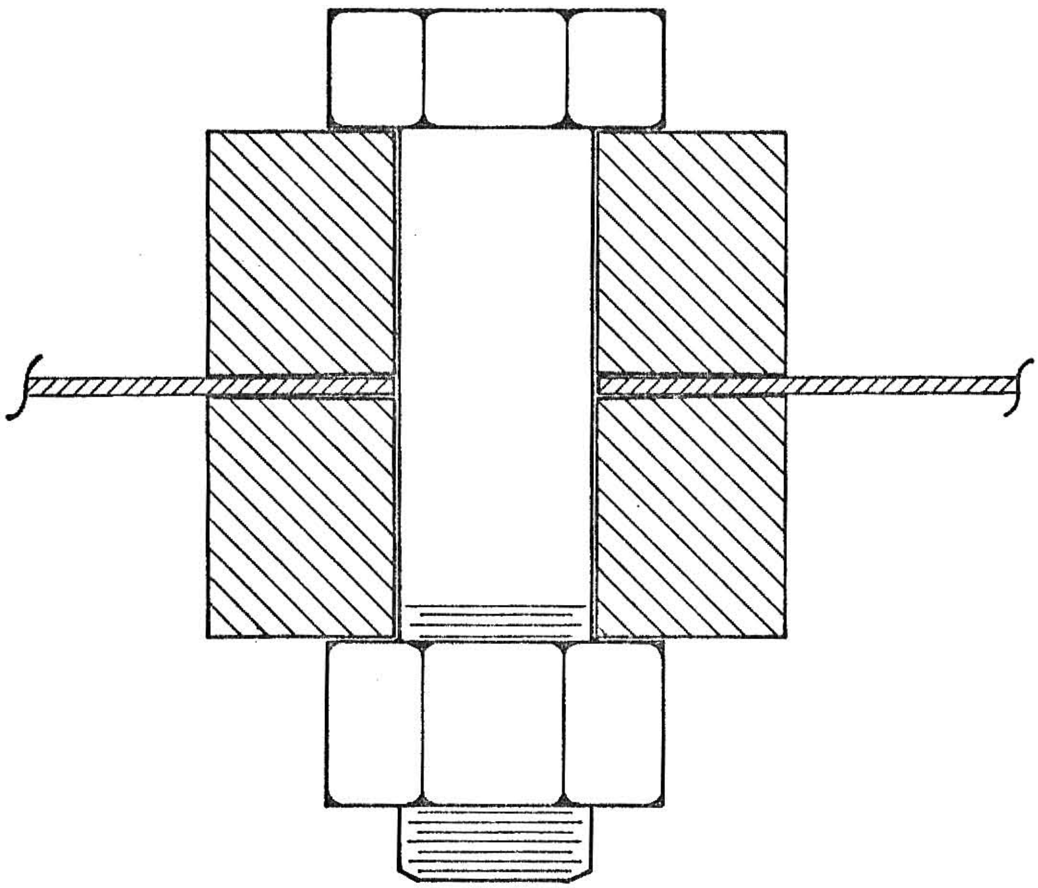

Fig. 15. Rigid Mass of Solid Cylindrical Design, Specimen B.

TABLE 7

Dimensions and Physical Properties of Test Specimens

Description	Magnitude	
	Specimen A	Specimen B
Outer Plate Radius	a = 5.045 in.	a = 5.045 in.
Plate Thickness	h = 0.037 in.	h = 0.037 in.
Radius Ratio	R = 0.150	R = 0.150
Mass Ratio	γ = 30.86	γ = 41.66
Modulus of Elasticity	E = 29 x 10^6 lb/in^2	E = 29 x 10^6 lb/in^2
Poissons Ratio	v = 0.3	v = 0.3
Mass Density	ρ = 0.00073 $lb\text{-}sec^2/in^4$	0.00073 $lb\text{-}sec^2/in^4$

plate was placed into a recessed ring bored from the face of the lower double flange, and the machined neck of the mating single flange was then placed on the plate in the recessed ring. Six 3/4-inch bolts extending through the outside faces of the flanges allowed the plate to be uniformly and rigidly clamped at its outer boundary. Hence, the boundary conditions of zero slope and zero radial and transverse deflection were modeled.

Through a rubber tipped driver centered on the rigid mass clamping bolt, an electrodynamic exciter forced the plate-mass test specimen into vibratory motion. The exciter was powered by a combination audio oscillator and power supply, mounted in the bottom rack of the control panel shown in Fig. 16. In the third rack from the top of the control panel, an electronic counter monitored the driving frequency and displayed it in digital form. The output from a velocity probe following the plate excursions and a combination oscillator velocity meter connection to an oscilloscope generated a Lissajous pattern for detection of the linear resonant frequency. The experimental apparatus and instrumentation used in the linear investigation is shown in Figs. 16 and 17. To study the nonlinear frequency-amplitude relationship, the equipment shown in Figs. 18, 19 and 20 was used. Mounted to a plexiglass support, the micrometer probe allowed measurement of the maximum excursions of the rigid center of the plate from its equilibrium position. The electronic counter was again used to display the frequency of the oscillator.

Experimental Procedure

Utilizing the equipment shown in Fig. 17, low power inputs to the exciter initiated small amplitude vibrations and provided a preliminary check on the linear resonant frequency. The velocity probe was then replaced by the micrometer and a measurement of the static equilibrium position of

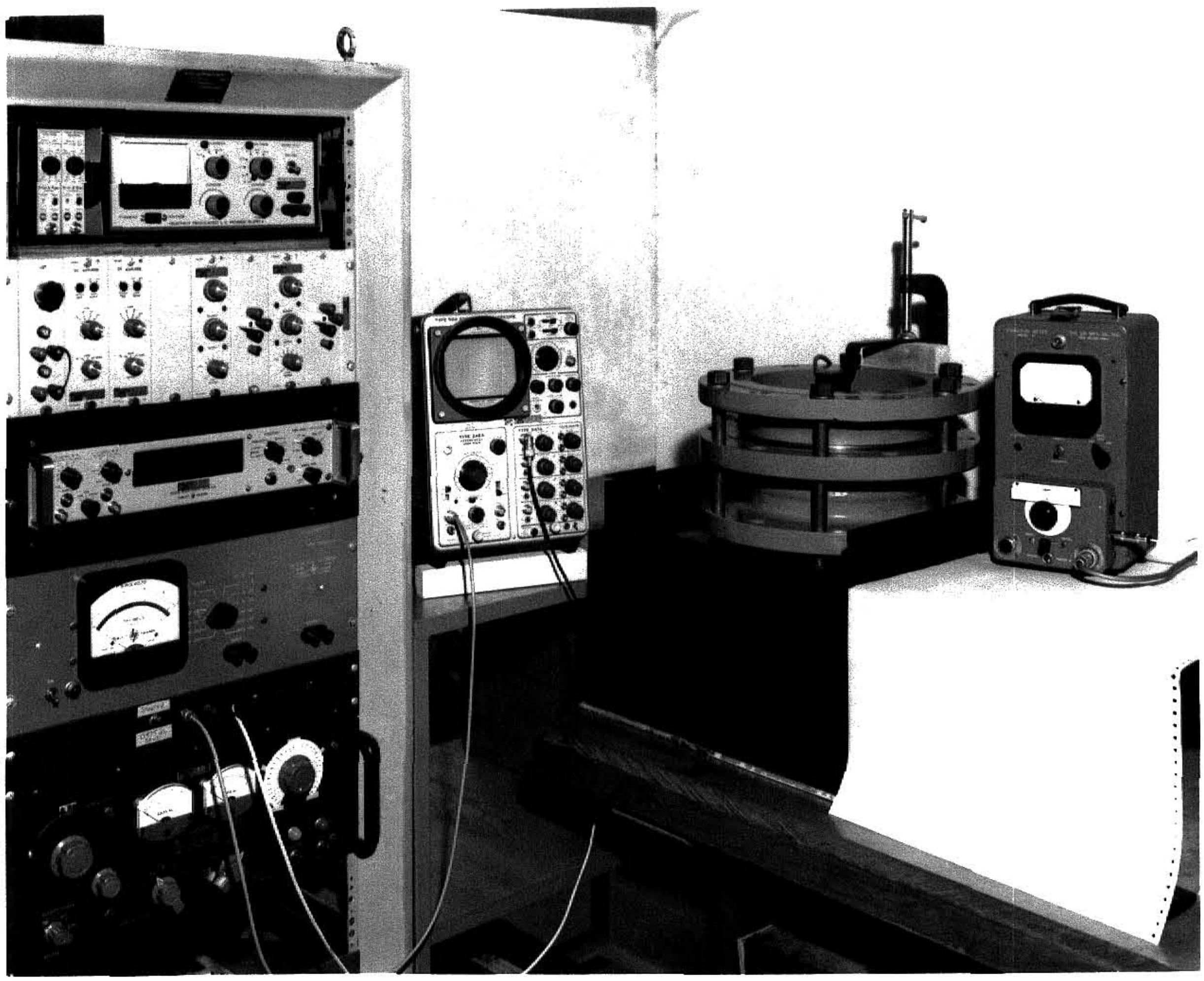

Fig. 16. Linear Test Apparatus and Instrumentation.

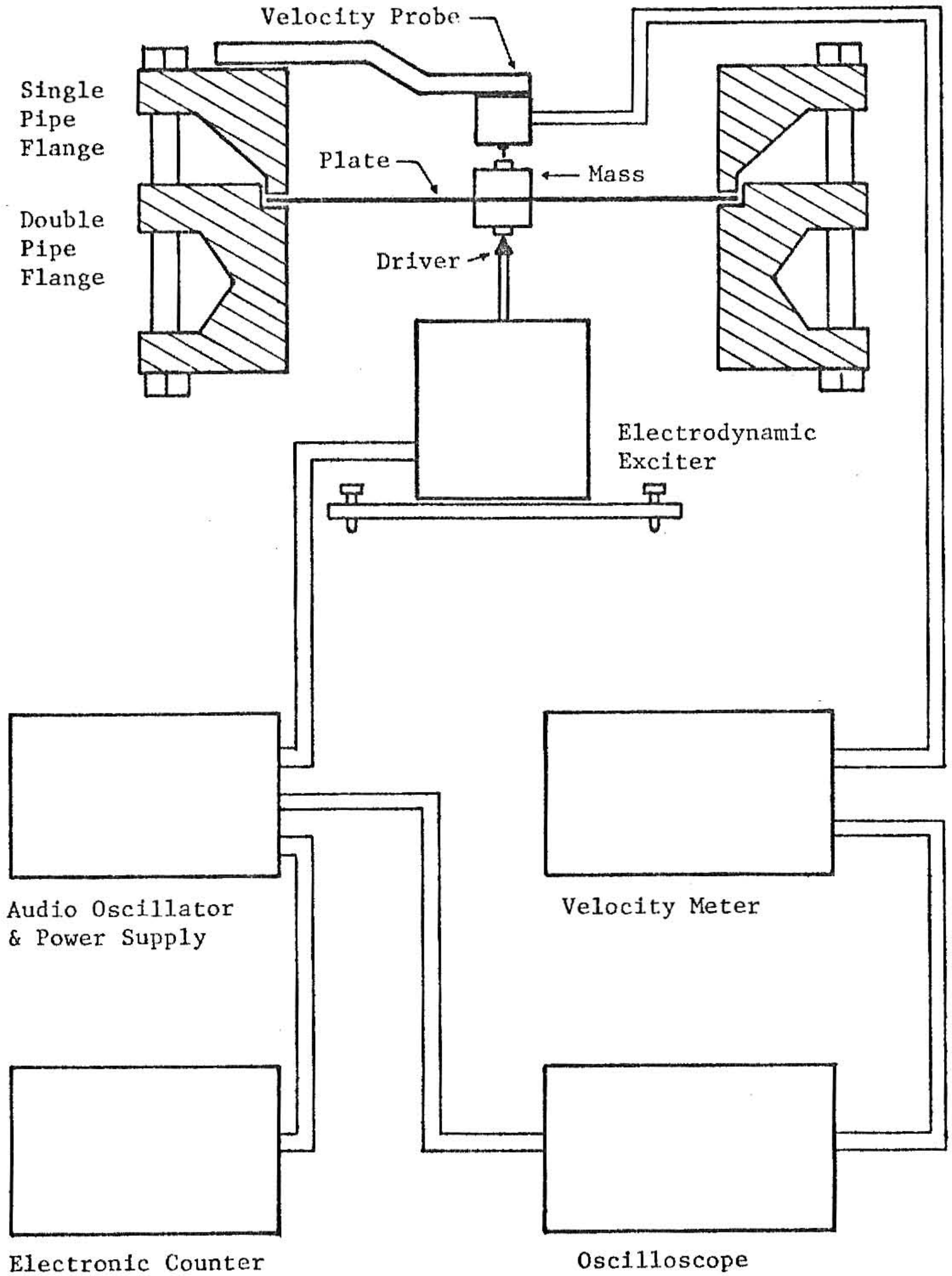

Fig. 17. Schematic of Linear Test Apparatus and Instrumentation.

Fig. 18. Nonlinear Test Apparatus and Instrumentation.

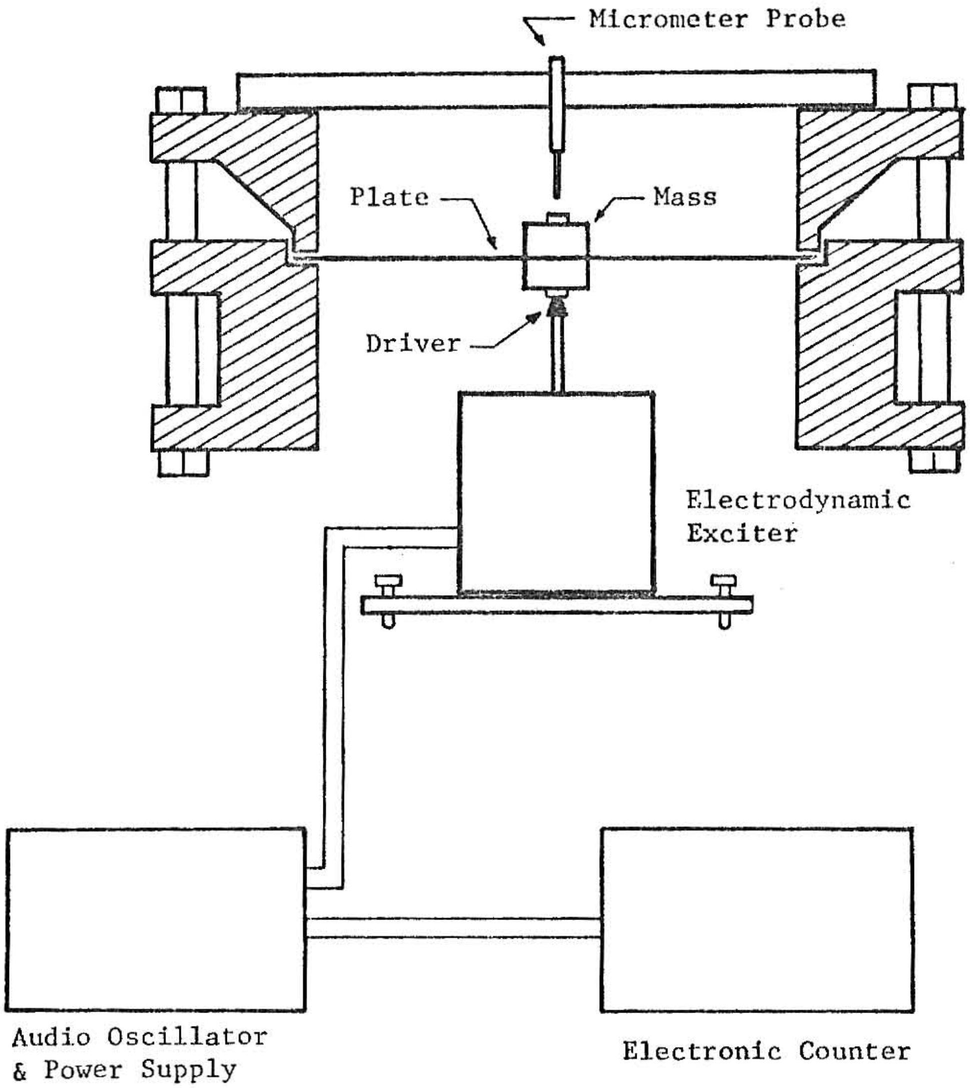

Fig. 19. Schematic of Nonlinear Test Apparatus and Instrumentation.

the plate was recorded. Holding the power input constant, the micrometer probe and frequency were adjusted simultaneously while seeking a driving frequency that resulted in a maximum amplitude of vibration. Slowly increasing the frequency through resonance many times, and each time readjusting the micrometer, the frequency corresponding to the maximum amplitude was determined. The amplitude was recorded at the micrometer adjustment which just prevented audible contact between the probe and the rigid center clamp. The difference between audible contact and no contact proved to be less than one thousandth of an inch, which was also the smallest scale division on the micrometer. Increasing the power input to the exciter, additional resonance points were determined until a sufficient set of damped natural frequencies and corresponding amplitudes were obtained to plot a resonance curve for relative amplitudes between zero and 2.0.

To assay the effectiveness and repeatability of the two clamping devices, both the plate and the rigid mass were released. The rigid mass was rotated relative to the plate, the plate was rotated with respect to the pipe flanges, and the test specimens were then reclamped before taking a second data set. A third test was conducted after turning the plate over in the pipe flange clamping fixture. The limited capabilities of the power supply and exciter influenced the choice of dimensions of the test specimens and hence also bounded the maximum attainable amplitudes. The relatively high mass ratios were selected to provide assurance that the theoretical boundary conditions at the inner radius were being closely modeled.

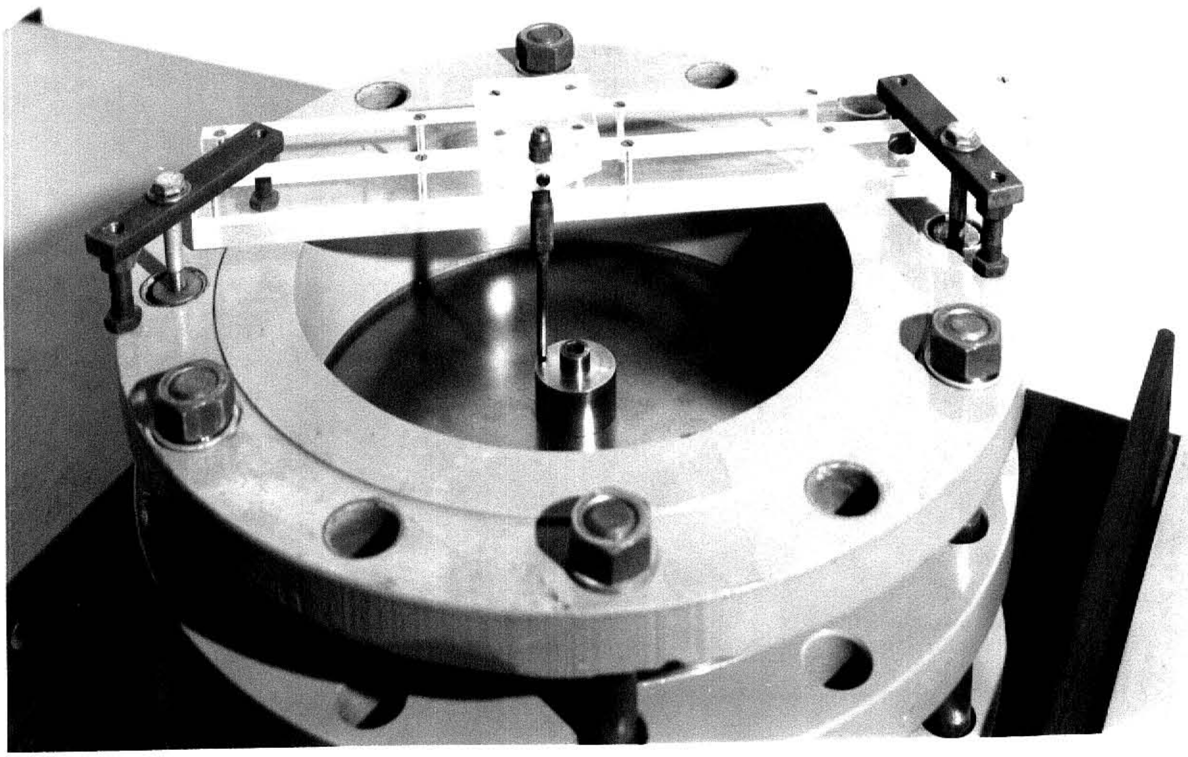

Fig. 20. Micrometer Probe and Test Specimen in Plate Clampling Fixture.

Experimental Results

Data obtained in the three successive tests on the two test specimens is given in Tables 8-13. Selected frequencies predicted by theory for the test specimens are given in Table 14. The two plate-mass systems with rigid centers of shell and solid design are labelled as Specimens A and B, respectively. Figures 21 and 22 compare the experimental data to the corresponding theoretical resonance curves which were drawn from values computed with Eq. (25) and the subsequently outlined numerical procedures. The frequency in cycles per second, Ω, and the dimensionless angular frequency, ω, are related by

$$\Omega = \frac{h\omega}{2\pi a^2}\sqrt{\frac{E}{12\rho(1-\nu^2)}} \tag{36}$$

In Tests I, II and III on each specimen, the experimental frequencies were found to be lower than that predicted by theory. Considering the unlikelihood of experimentally achieving ideally clamped plate boundaries, the lower frequencies are not unexpected nor unreasonably displaced from theory. Since the data was taken for increasing frequencies, reference to the behavior of a nonlinear system undergoing forced vibrations provides an additional explanation for the lower frequencies. The shifts in frequency between the three consecutive tests are most likely due to an inability to clamp the plate in precisely the same manner for each test. However, the reproducibility of the experimental results is demonstrated to a limited extent by the parallelism of the data for each of the three tests, and by its conformity to the shape of the theoretical curve at low amplitudes. A further comparison of the experimental data with the theoretical resonance reveals a presently unexplained phenomenon. Although the theoretical and experimental curves are nearly parallel at low amplitudes, beyond relative amplitudes near $W_R/h = 1.0$, the test data exhibits a bend more to the right than that predicted by theory. At increasing amplitudes, the experimental values return such that the curves are again nearly parallel. Attributing this slight depression in the experimental curves to a failure in clamping the plate boundaries may prove to be an erroneous conclusion. Reference to the experimental data presented by Sandman [14], for the nonlinear response of an annular plate reveals a strikingly similar depression near the same portion of the response curve. Likewise, data given by Kung and Pao [15], for the nonlinear response of a circular plate also exhibits the depression. These similarities in the independent investigations serve to preclude any premise that the phenomenon is due to failure of the clamping devices, and instead suggests that the non-parallelism of theory and experiment at large amplitudes may be due to neglection of significant factors in the theoretical derivations. A contribution to the observed phenomena could possibly arise from the basic assumptions which neglect the coupling of higher modes. Notably, when amplitudes near $W_R/h = 2.5$ were induced during the experimental investigation, unsymmetrical vibration of the rigid center was visually detectable.

TABLE 8

Data for Test I, Specimen A

Frequency cps	Micrometer Reading, in.	Deflection in.	W_R/h
0	0.196	0	0
70.1	0.190	0.006	.162
70.9	0.184	0.012	.324
72.4	0.179	0.017	.459
74.5	0.174	0.022	.595
76.8	0.168	0.028	.757
80.3	0.162	0.034	.919
84.2	0.157	0.039	1.054
88.2	0.153	0.043	1.162
91.3	0.150	0.046	1.243
94.4	0.145	0.051	1.378
96.7	0.141	0.055	1.486
100.1	0.137	0.059	1.595
103.8	0.134	0.062	1.676
108.6	0.129	0.067	1.811
113.0	0.124	0.072	1.946

TABLE 9

Data for Test II, Specimen A

Frequency cps	Micrometer Reading, in.	Deflection in.	W_R/h
0	0.173	0	0
71.5	0.169	0.004	0.108
72.4	0.163	0.010	0.270
74.3	0.156	0.017	0.459
77.1	0.150	0.023	0.622
79.7	0.144	0.029	0.784
85.0	0.138	0.035	0.946
89.1	0.133	0.040	1.081
92.6	0.129	0.044	1.189
96.2	0.124	0.049	1.324
99.8	0.118	0.055	1.486
102.1	0.115	0.058	1.568
104.7	0.111	0.062	1.676
107.4	0.107	0.066	1.784
111.4	0.103	0.070	1.892

TABLE 10

Data for Test III, Specimen A

Frequency cps	Micrometer Reading, in.	Deflection in.	W_R/h
0	0.181	0	0
68.5	0.176	0.005	0.135
69.3	0.170	0.011	0.297
70.7	0.163	0.018	0.486
73.0	0.157	0.024	0.649
77.0	0.149	0.032	0.865
80.1	0.143	0.038	1.027
82.8	0.139	0.042	1.135
85.9	0.135	0.046	1.243
90.5	0.130	0.051	1.378
93.5	0.127	0.054	1.459
97.0	0.124	0.057	1.541
101.4	0.120	0.061	1.649
105.2	0.116	0.065	1.757
109.0	0.112	0.069	1.865
111.5	0.108	0.073	1.973

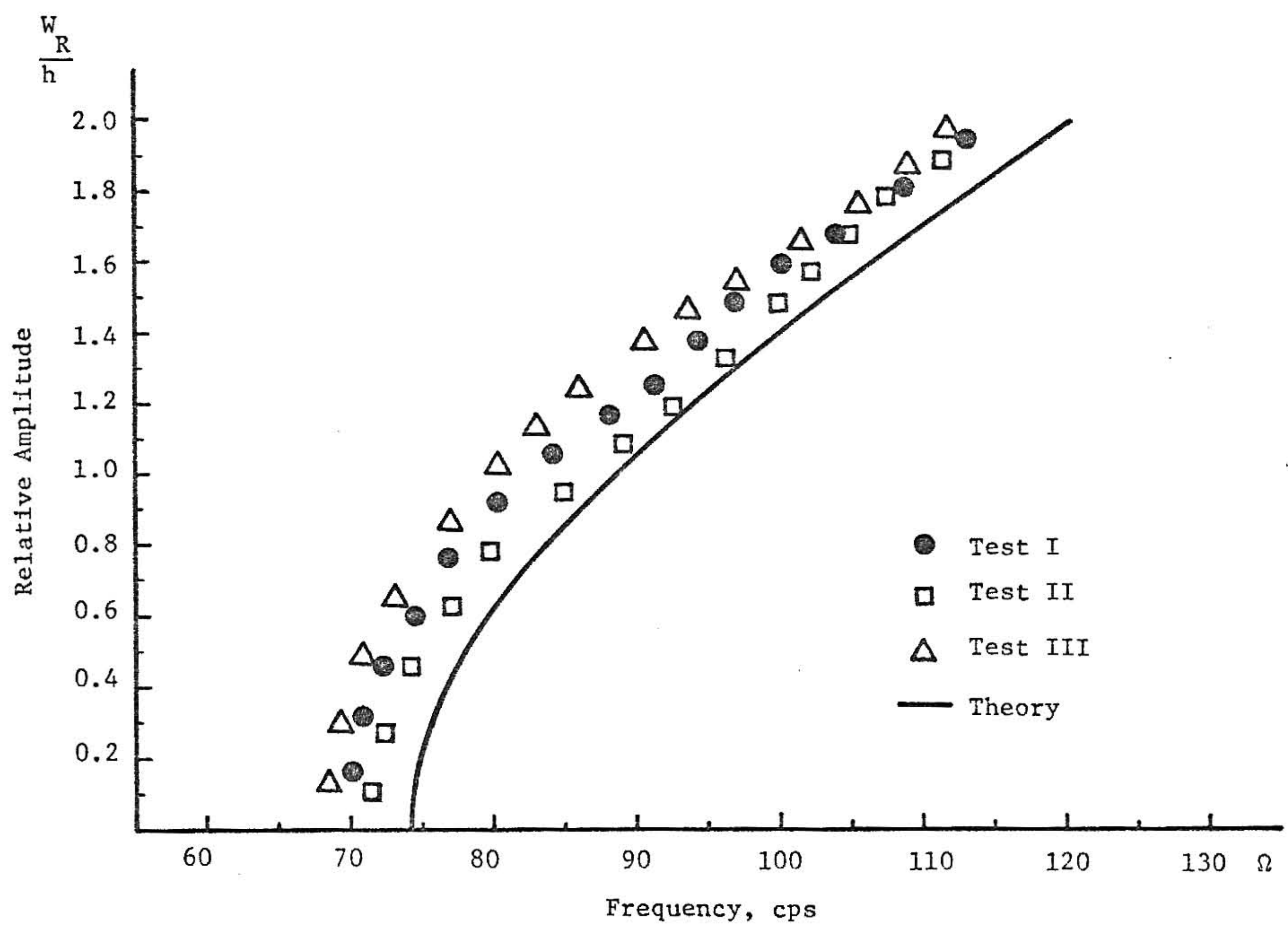

Fig. 21. Comparison of Experimental and Theoretical Resonance of Specimen A.

TABLE 11

Data for Test I, Specimen B

Frequency cps	Micrometer Reading, in.	Deflection in.	W_R/h
0	0.287	0	0
62.6	0.283	0.004	0.108
64.4	0.276	0.011	0.297
66.6	0.269	0.018	0.486
68.7	0.263	0.024	0.649
72.1	0.257	0.030	0.811
75.5	0.251	0.036	0.973
78.8	0.245	0.042	1.135
81.7	0.241	0.046	1.243
84.7	0.238	0.049	1.324
88.2	0.234	0.053	1.432
90.4	0.229	0.058	1.568
94.0	0.224	0.063	1.703
97.9	0.220	0.067	1.811
100.8	0.216	0.071	1.919

TABLE 12

Data for Test II, Specimen B

Frequency cps	Micrometer Reading, in.	Deflection in.	W_R/h
0.	0.284	0	0
61.5	0.278	0.006	0.162
62.4	0.272	0.012	0.324
63.9	0.267	0.017	0.459
65.7	0.262	0.022	0.595
68.4	0.255	0.029	0.784
71.9	0.250	0.034	0.919
75.8	0.244	0.040	1.081
79.0	0.240	0.044	1.189
81.9	0.237	0.047	1.270
85.3	0.232	0.052	1.405
88.2	0.226	0.058	1.568
90.6	0.223	0.061	1.649
94.6	0.218	0.066	1.784
100.4	0.211	0.073	1.973

TABLE 13

Data for Test III, Specimen B

Frequency cps	Micrometer Reading, in.	Deflection in.	W_R/h
0	0.317	0	0
60.3	0.310	0.007	0.189
61.7	0.304	0.013	0.351
62.8	0.298	0.019	0.514
66.0	0.291	0.026	0.703
68.4	0.286	0.031	0.838
70.6	0.281	0.036	0.973
73.5	0.277	0.040	1.081
76.3	0.272	0.045	1.216
80.4	0.268	0.049	1.324
84.1	0.263	0.054	1.459
86.7	0.259	0.058	1.568
90.8	0.252	0.065	1.757
93.6	0.249	0.068	1.838
97.1	0.245	0.072	1.946

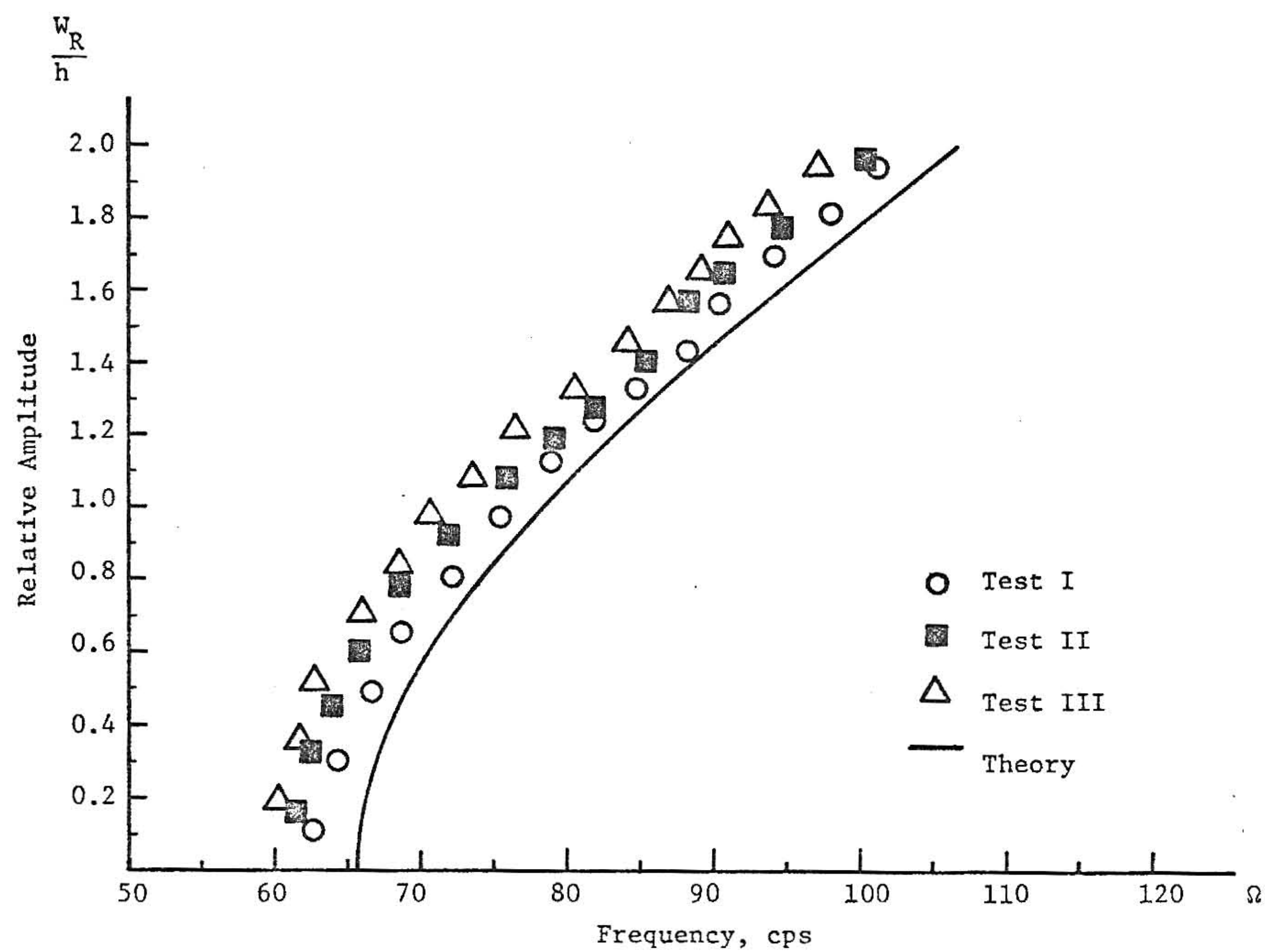

Fig. 22. Comparison of Experimental and Theoretical Resonance of Specimen B.

TABLE 14

Predicted Frequencies of Test Specimens
Ω, cps

W_R/h \ γ	Specimen A 30.86	Specimen B 41.66
0.0	74.2	65.7
0.4	76.7	67.9
0.8	83.8	74.1
1.2	94.1	83.2
1.6	106.5	94.2

DISCUSSION AND CONCLUSION

The merit of the energy method derivation is that both the governing differential equations and the natural boundary conditions are obtained simultaneously. By assuming the existence of harmonic oscillations, the proposed wave forms (18) permit retention of the terms of the so-called second strain invariant and allows reduction of von Karman's dynamic equations to a related set of initial value problems for which a solution is obtainable via a numerical integration technique. Although the assumed wave forms appear to contradict the inseparability of modes inherent in the coupled equations, physical arguments as well as recent studies [13,16] demonstrate the excellent suitability of the assumed wave forms. The method used can be easily extended to investigate forced vibrations, alternate boundary conditions and stress distributions.

The discrepencies discovered in the nonlinear frequencies predicted by Berger's equations and the more rigorous von Karman equations appears to be related to both the completeness of the theory and the treatment of the boundary conditions. Cognizant of these differences in theory, recognizing the limitations of the theoretical derivations, and recalling the unexplained phenomenon observed in the experimental investigations, it appears that present theory should not be extended beyond relative amplitudes of 2.0. Near that amplitude, errors of sufficient magnitude are introduced to demand further investigation and more reliable frequency predictions. It has also been demonstrated that the use of Berger's simplifications may lead to significantly different results when applied to nonlinear plate vibrations. Thus, a further study of the physical significance of Berger's assumptions would be of considerable value in determining when the simplifying assumptions are applicable.

The methods employed in this investigation are supported by the excellent agreement with prior nonlinear predictions when the present problem was reduced to approximate a flat circular plate. Likewise, linearization of the problem afforded an additional check on the procedure. An experimental investigation offered further verification of the nonlinear response curves predicted. Hence, the results provided by the analytical and numerical procedures employed in this investigation proved to be reliable predictors of both the linear and nonlinear responses of plate-mass systems. As such, they should be of considerable value to designers as well as to those seeking to improve upon related theory.

Since vibrations may be disastrous as well as useful, reliable predictors of their nature are of considerable importance. Vibration may result in deflections of sufficient magnitude to cause malfunction of important components. Associated high stresses may lead to decreased life through increased material fatigue, and undesirable noise accompanying the vibration may produce human discomfort as well. Therefore, the information offered in Figs. 3-12 is of considerable use to a designer attempting to predict or alter the frequency response of a circular component containing a concentric rigid inclusion. The discovered changes in response associated with a change in the dimensions are not easily predicted intuitively, and thus the information provided herein could prevent inadvertantly achieving results contrary to those desired.

REFERENCES

1. Langhaar, H. L., Energy Methods in Applied Mechanics, John Wiley and Sons, 1962, pp. 159-198.

2. Berger, H. M., "A New Approach to the Analysis of Large Deflections of Plates," J. Appl. Mech., Vol. 22, Trans. ASME, Vol. 77, 1955, pp. 465-472.

3. Handelman, G. and Cohen, H., "On the effects of the Addition of Mass to Vibrating Systems," Proc. 9th Int. Con. Appl. Mech., Vol. 7, 1957, pp. 509-516.

4. Chiang, D. C. and Chen, S. S. H., "Large Amplitude Vibration of a Circular Plate with Concentric Rigid Mass," J. Appl. Mech., Vol. 39, No. 2, Trans. ASME, Vol. 94, 1972, pp. 577-584.

5. Nowinski, J. L. and Ohnabe, H., "On Certain Inconsistencies in Berger Equations for Large Deflections of Elastic Plates," Int. J. Mech. Sci., Vol. 14, No. 3, 1972, pp. 165-170.

6. Ramachandran, J., "Nonlinear Vibrations of a Rectangular Plate Carrying a Concentrated Mass," J. Appl. Mech., Vol. 40, No. 2, Trans. ASME, 1973, pp. 630-632.

7. Sandman, B. E. and Huang, C.-L., "Large Amplitude Vibrations of a Rigidly Clamped Circular Plate," Int. J. Non-Linear Mech., Vol. 6, 1971, pp. 451-468.

8. Timoshenko, S. and S. Woinowsky-Kreiger, Theory of Plates and Shells, 2nd edn., McGraw-Hill, 1959, pp. 396-428.

9. Sokolnikoff, I. S., Mathematical Theory of Elasticity, 2nd Edn., McGraw-Hill, 1956, pp. 421-425.

10. Kantorovich, L. V. and Krylov, V. I., Approximate Methods of Higher Analysis, Interscience Publishers, Inc., 1958.

11. Timoshenko, S. and Young, D. H., Advanced Dynamics, McGraw-Hill, 1948, pp. 233-236.

12. Keller, H. B., Numerical Methods for Two-Point Boundary-Value Problems Blaisdell Publ. Co., 1968.

13. Huang, C.-L. and Sandman, B. E., "Finite Amplitude Oscillations of a Thin Elastic Annulus," Proc. 12th Midwestern Mechanics Conference, University of Notre Dame, 1971, p. 921.

14. Sandman, B. E., Harmonic Oscillations of Circular and Annular Plates at Finite Amplitudes, Ph.D. Dissertation, Kansas State University, Manhattan, Kansas, 1970.

15. Kung, G. C. and Pao, Y.-H., "Nonlinear Flexural Vibrations of a Clamped Circular Plate," J. Appl. Mech., Vol. 39, No. 4, Trans. ASME, 1972, pp. 1050-1054.

16. Walker, H. S. and Sandman, B. E., "An Experimental Observation in Large Amplitude Plate Vibrations," J. Appl. Mech., Vol. 40, No. 2, 1973, pp. 633-634.

The first variation δI of the action integral is found to be

$$\delta I = -2\pi\rho h\varepsilon \int_{t_0}^{t_1} \int_b^a r\, w_{tt}\, \eta \, drdt \tag{37}$$

$$- \varepsilon \int_{t_0}^{t_1} M\, w_{tt}\, \eta(b,t)\Big|_{r=b} dt$$

$$- 2\pi D\varepsilon \int_{t_0}^{t_1} r(w_{rr} + \frac{\nu}{r} w_r)\eta_r\Big|_b^a dt$$

$$+ 2\pi D\varepsilon \int_{t_0}^{t_1} r(w_{rrr} + \frac{w_{rr}}{r} - \frac{w_r}{r^2})\eta\Big|_b^a dt$$

$$- 2\pi D\varepsilon \int_{t_0}^{t_1} \int_b^a r(w_{rrrr} + \frac{2}{r} w_{rrr} - \frac{w_{rr}}{r^2} + \frac{w_r}{r^3})\eta \, drdt$$

$$- \frac{24\pi D}{h^2} \varepsilon \int_{t_0}^{t_1} r(u_r + \frac{w_r^2}{2} + \frac{\nu u}{r})\zeta\Big|_b^a dt$$

$$- \frac{24\pi D}{h^2} \varepsilon \int_{t_0}^{t_1} rw_r(u_r + \frac{w_r^2}{2} + \frac{\nu u}{r})\eta\Big|_b^a dt$$

$$+ \frac{24\pi D}{h^2} \varepsilon \int_{t_0}^{t_1} \int_b^a r(u_{rr} + \frac{u_r}{r} + w_r w_{rr} + \frac{w_r^2}{2r} + \frac{\nu u_r}{r})\zeta \, drdt$$

$$+ \frac{24\pi D}{h^2} \varepsilon \int_{t_0}^{t_1} \int_b^a r(u_r w_{rr} + u_{rr} w_r + \frac{u_r}{r} w_r + \frac{3}{2} w_r^2 w_{rr} + \frac{w_r^3}{2r}$$

$$+ \frac{\nu u}{r} w_{rr} + \frac{\nu}{r} u_r w_r)\eta \, drdt$$

$$- \frac{24\pi D}{h^2} \varepsilon \int_{t_0}^{t_1} \int_b^a r(\frac{\nu u_r}{r} + \frac{\nu w_r^2}{2r} + \frac{u}{r^2})\zeta \, drdt$$

APPENDIX B

Differentiation of the initial value problem with respect to η_1, η_2, and λ yields the variational problem defined by Eqs. (35a), (35c), and (35e), as follows:

Variational Equations

$$\left.\begin{aligned}
\frac{d}{d\xi}\left(\frac{\partial z_1}{\partial \eta_1}\right) &= \frac{\partial z_2}{\partial \eta_1} \\
\frac{d}{d\xi}\left(\frac{\partial z_2}{\partial \eta_1}\right) &= \frac{\partial z_3}{\partial \eta_1} \\
\frac{d}{d\xi}\left(\frac{\partial z_3}{\partial \eta_1}\right) &= \frac{\partial z_4}{\partial \eta_1} \\
\frac{d}{d\xi}\left(\frac{\partial z_4}{\partial \eta_1}\right) &= -\frac{2}{\xi}\left(\frac{\partial z_4}{\partial \eta_1}\right) + \frac{1}{\xi^2}\left(\frac{\partial z_3}{\partial \eta_1}\right) - \frac{1}{\xi^3}\left(\frac{\partial z_2}{\partial \eta_1}\right) + \lambda\left(\frac{\partial z_1}{\partial \eta_1}\right) \\
&\quad + \frac{9(1-\nu^2)\alpha}{\xi}\left[z_3\left(\frac{\partial z_5}{\partial \eta_1}\right) + z_5\left(\frac{\partial z_3}{\partial \eta_1}\right) + z_2\left(\frac{\partial z_6}{\partial \eta_1}\right) + z_6\left(\frac{\partial z_2}{\partial \eta_1}\right)\right] \\
\frac{d}{d\xi}\left(\frac{\partial z_5}{\partial \eta_1}\right) &= \frac{\partial z_6}{\partial \eta_1} \\
\frac{d}{d\xi}\left(\frac{\partial z_6}{\partial \eta_1}\right) &= -\frac{1}{\xi}\left(\frac{\partial z_6}{\partial \eta_1}\right) + \frac{1}{\xi^2}\left(\frac{\partial z_5}{\partial \eta_1}\right) - \frac{1}{\xi}\, z_2\left(\frac{\partial z_2}{\partial \eta_1}\right)
\end{aligned}\right] \qquad (38a)$$

$$\left.\begin{aligned}
\frac{d}{d\xi}\left(\frac{\partial z_1}{\partial \eta_2}\right) &= \frac{\partial z_2}{\partial \eta_2} \\
\frac{d}{d\xi}\left(\frac{\partial z_2}{\partial \eta_2}\right) &= \frac{\partial z_3}{\partial \eta_2} \\
\frac{d}{d\xi}\left(\frac{\partial z_3}{\partial \eta_2}\right) &= \frac{\partial z_4}{\partial \eta_2}
\end{aligned}\right] \qquad (38b)$$

$$\frac{d}{d\xi}\left(\frac{\partial z_4}{\partial \eta_2}\right) = -\frac{2}{\xi}\left(\frac{\partial z_4}{\partial \eta_2}\right) + \frac{1}{\xi^2}\left(\frac{\partial z_3}{\partial \eta_2}\right) - \frac{1}{\xi^3}\left(\frac{\partial z_2}{\partial \eta_2}\right) + \lambda\left(\frac{\partial z_1}{\partial \eta_2}\right)$$

$$+ \frac{9(1-\nu^2)\alpha}{\xi}\left[z_3\left(\frac{\partial z_5}{\partial \eta_2}\right) + z_5\left(\frac{\partial z_3}{\partial \eta_2}\right) + z_2\left(\frac{\partial z_6}{\partial \eta_2}\right) + z_6\left(\frac{\partial z_2}{\partial \eta_2}\right)\right]$$

$$\frac{d}{d\xi}\left(\frac{\partial z_5}{\partial \eta_2}\right) = \frac{\partial z_6}{\partial \eta_2}$$

$$\frac{d}{d\xi}\left(\frac{\partial z_6}{\partial \eta_2}\right) = -\frac{1}{\xi}\left(\frac{\partial z_6}{\partial \eta_2}\right) + \frac{1}{\xi^2}\left(\frac{\partial z_5}{\partial \eta_2}\right) - \frac{1}{\xi} z_2\left(\frac{\partial z_2}{\partial \eta_2}\right)$$

$$\frac{d}{d\xi}\left(\frac{\partial z_1}{\partial \lambda}\right) = \frac{\partial z_2}{\partial \lambda}$$

$$\frac{d}{d\xi}\left(\frac{\partial z_2}{\partial \lambda}\right) = \frac{\partial z_3}{\partial \lambda}$$

$$\frac{d}{d\xi}\left(\frac{\partial z_3}{\partial \lambda}\right) = \frac{\partial z_4}{\partial \lambda}$$

$$\frac{d}{d\xi}\left(\frac{\partial z_4}{\partial \lambda}\right) = -\frac{2}{\xi}\left(\frac{\partial z_4}{\partial \lambda}\right) + \frac{1}{\xi^2}\left(\frac{\partial z_3}{\partial \lambda}\right) - \frac{1}{\xi^3}\left(\frac{\partial z_2}{\partial \lambda}\right) + \lambda\left(\frac{\partial z_1}{\partial \lambda}\right) \tag{38c}$$

$$+ \frac{9(1-\nu^2)\alpha}{\xi}\left[z_3\left(\frac{\partial z_5}{\partial \lambda}\right) + z_5\left(\frac{\partial z_3}{\partial \lambda}\right) + z_2\left(\frac{\partial z_6}{\partial \lambda}\right) + z_6\left(\frac{\partial z_2}{\partial \lambda}\right)\right]$$

$$+ z_1$$

$$\frac{d}{d\xi}\left(\frac{\partial z_5}{\partial \lambda}\right) = \frac{\partial z_6}{\partial \lambda}$$

$$\frac{d}{d\xi}\left(\frac{\partial z_6}{\partial \lambda}\right) = -\frac{1}{\xi}\left(\frac{\partial z_6}{\partial \lambda}\right) + \frac{1}{\xi^2}\left(\frac{\partial z_5}{\partial \lambda}\right) + \frac{1}{\xi} z_2\left(\frac{\partial z_2}{\partial \lambda}\right)$$

ACKNOWLEDGMENT

The author wishes to give special recognition to his major professor, Dr. Hugh S. Walker, whose guidance, contributions and encouragement throughout the preparation of this thesis was especially appreciated.

Acknowledgment is due Dr. Chi-Lung Huang for his helpful and enthusiastic counsel on theoretical considerations. The author also offers his thanks to Mr. Wallace M. Johnston for providing technical skill in machining parts of the experimental apparatus.

VITA

The author was born in LaCrosse, Kansas, November 28, 1948, the son of Julius C. and Ann M. Becker.

He attended High Prarie Grade School in Osborne County and Downs High School in Downs, Kansas. Following graduation in 1966, he enrolled at Kansas State University. As an undergraduate, he worked for Phillips Petroleum Company while participating in the Engineering Co-op Program. He was employed part-time as an assistant in the Engineering Materials Lab of the Industrial Engineering Department and as a research aide in the Applied Mechanics Department. In December 1971, he received a B.S. in Mechanical Engineering and was accepted in the Graduate School of Mechanical Engineering at K.S.U. where he was the recipient of an NDEA Fellowship, served as a graduate teaching assistant and was appointed an Instructor in the Mechanical Engineering Department in the fall of 1974. The author is a member of Pi Tau Sigma, an Associate Member of ASME, and is employed in an engineering capacity between academic sessions by Becker Mfg. Co., Inc.

NONLINEAR VIBRATIONS OF A CLAMPED CIRCULAR PLATE CARRYING A CONCENTRIC RIGID MASS

by

LeWayne Carl Becker

B.S., Kansas State University, 1971

AN ABSTRACT OF A MASTER'S THESIS

submitted in partial fulfillment of the

requirements for the degree

MASTER OF SCIENCE

Department of Mechanical Engineering

KANSAS STATE UNIVERSITY
Manhattan, Kansas

1975

ABSTRACT

Large amplitude vibrations of circular plates with attached concentric rigid masses are investigated. The problem is formulated in terms of von Karman's dynamic equations by Hamilton's Principle. Harmonic oscillations are assumed and the time variable is eliminated by a time averaging method. The resulting ordinary nonlinear differential equations of motion form a boundary-value problem. Numerical results are obtained by introducing the related initial-value problem and successive corrections and perturbations of the parameters, provide approximate solutions to the boundary-value problem. The nonlinear vibration characteristics are investigated for various mass and radii ratios, and the results agree with those of the classical linear solution when the amplitude of vibration tends to zero. Agreement with prior work is also obtained for large amplitude vibrations of a flat circular plate when the radius of the rigid mass tends to zero and a mass ratio of unity is prescribed. Experimental observations of the plate-mass system also support the method of solution. Considerable disagreements with the nonlinear response predicted by Berger's simplified equations are noted.